

## Synthetic hydrogels identify matrix physicochemical properties required for renal epithelial cell tubulogenesis

**Authors:** Ricardo Cruz-Acuña<sup>1,2</sup>, Adriana Mulero-Russe<sup>2,3</sup>, Amy Y. Clark<sup>2,4</sup>, Roy Zent<sup>5</sup>, and Andrés J. García<sup>2,4</sup>

### Affiliations:

<sup>1</sup>Wallace H. Coulter Department of Biomedical Engineering, Georgia Institute of Technology, Atlanta, GA 30332

<sup>2</sup>Parker H. Petit Institute for Bioengineering and Biosciences, Georgia Institute of Technology, Atlanta, GA 30332

<sup>3</sup>School of Chemical & Biomolecular Engineering, Georgia Institute of Technology, Atlanta, GA 30332

<sup>4</sup>George W. Woodruff School of Mechanical Engineering, Georgia Institute of Technology, Atlanta, GA 30332

<sup>5</sup>Department of Medicine, Vanderbilt University, Nashville, TN 37235

### Corresponding author:

A.J. García (andres.garcia@me.gatech.edu)

### Abstract

Synthetic hydrogels with controlled physicochemical matrix properties serve as powerful *in vitro* tools to dissect cell-extracellular matrix (ECM) interactions that regulate epithelial morphogenesis in 3D microenvironments. In addition, these fully defined matrices overcome the lot-to-lot variability of naturally-derived materials and have provided insights into the formation of rudimentary epithelial organs. Therefore, we engineered a fully defined, synthetic hydrogel with independent control over proteolytic degradation, mechanical properties, and adhesive ligand type and density to study the impact of ECM properties on epithelial tubulogenesis for inner medullary collecting duct (IMCD) cells. Protease sensitivity of the synthetic material for membrane-type matrix metalloproteinase-1 (MT1-MMP) was

required for tubulogenesis. Additionally, a defined range of matrix elasticity and presentation of RGD adhesive peptide at a threshold level of 2 mM ligand density were required for epithelial tubulogenesis. Finally, we demonstrated that the engineered hydrogel supported organization of epithelial tubules with a lumen and secreted laminin. This synthetic hydrogel serves as a platform that supports epithelial tubular morphogenetic programs and can be tuned to identify ECM biophysical and biochemical properties required for epithelial tubulogenesis.

## Introduction

The extracellular matrix (ECM) provides mechanical and biochemical signals that modulate diverse morphogenetic processes such as renal epithelial morphogenesis<sup>1,2</sup>. For instance, the ECM provides physical support for the three-dimensional (3D) spatial organization of renal epithelial cells into tubular structures. Additionally, interactions between ECM components and integrin receptors regulate mechanotransduction pathways and modulate the activity of signaling molecules (e.g. Wnt family) that mediate the formation of polarized and differentiated epithelia<sup>1,3</sup>. In order to understand the contributions of the ECM to epithelial tubulogenesis, 3D collagen gels and Matrigel<sup>TM</sup> have been used in organotypic cultures that recreate the epithelial morphogenetic developmental program<sup>4,5</sup>. In these biological matrices, murine inner medullary collecting duct (IMCD) cells proliferate from single cells to form multicellular tubular or spheroidal structures when cultured in collagen gel or Matrigel<sup>TM</sup>, respectively, recapitulating the morphogenetic program of rudimentary epithelial renal structures<sup>6-9</sup> (Supplementary Fig. 1a,b). However, these biological matrices are inherently limited by lot-to-lot compositional and structural variability as well as the inability to decouple biochemical and biomechanical properties<sup>10,11</sup>. For instance, changes to the bulk concentration (e.g. increase matrix density) of collagen gels is a common approach to vary its mechanical properties (Supplementary Fig. 1c). However, these changes in collagen concentration unavoidably alter other matrix properties, such as adhesive ligand density and fiber density/structure<sup>12</sup>. Although modulation of bulk concentration of collagen gels results in changes in IMCD projected area and longest distance between two points along the projected area (Feret diameter; Supplementary Fig. 1d,e), it is unknown whether this effect is mediated by differences in biochemical or biomechanical matrix properties between different collagen gel formulations. Furthermore, in the case of Matrigel<sup>TM</sup>, its tumor-derived nature limits its translational potential<sup>11,12</sup>, establishing a need for a well-defined, tunable biomaterial that recapitulates the role of ECM properties on epithelial morphogenesis with potential for translational therapies. These limitations can be addressed by engineering synthetic hydrogel

systems that allow independent control over physicochemical properties to dissect the independent contributions of matrix biophysical and biochemical properties to epithelial morphogenesis<sup>13-15</sup>. These hydrogel systems facilitate the modeling and analysis of cell developmental processes while dissecting the specific microenvironmental signals that are essential for morphogenesis<sup>14,16-18</sup>, and serve as platforms to model human epithelial developmental programs with clinical translational potential<sup>13,19,20</sup>. For example, a synthetic material containing animal-derived heparin that supports epithelial tubulogenesis programs has been described as an alternative to biological matrices<sup>21</sup>.

Here, we describe a fully-defined, synthetic hydrogel that supports epithelial tubulogenesis of IMCD cells without the use of naturally-derived materials. Protease sensitivity, matrix elasticity, and adhesive peptide type and density of the synthetic hydrogel were important parameters in engineering a fully-synthetic matrix that supports the IMCD cell tubulogenesis program. The modular design of this synthetic matrix allows the study of the independent contributions of physicochemical matrix properties to IMCD cell tubulogenesis and overcomes limitations associated with biological matrices.

## Results

### *PEG-4MAL hydrogel supports MT1-MMP-directed tubule formation in a polymer density-dependent manner*

We selected a hydrogel platform based on four-armed, maleimide-terminated poly(ethylene glycol) (PEG-4MAL) macromer units that present elements inspired by the ECM such as cell adhesion peptides and matrix metalloproteinase (MMP)-sensitive crosslinking peptides (Supplementary Fig. 2a). Although other synthetic hydrogel systems have been developed to mimic properties of biological ECM, the PEG-4MAL hydrogel platform has significant advantages including well-defined structure, stoichiometric incorporation of bioactive molecules, increased cytocompatibility, and improved crosslinking efficiency<sup>2,16,20,22,23</sup>. In addition, the tunable properties of PEG-4MAL hydrogels allow the study of the independent contributions of biophysical and biochemical matrix properties for both single and collective epithelial cell programs<sup>2,20</sup>. For instance, using this platform we showed that normal epithelial cyst growth, polarization, and lumen formation for Madin-Darby canine kidney (MDCK) cells are restricted to a narrow range of matrix elasticity, required a threshold level of cell-directed matrix degradability, and were dramatically regulated by adhesive peptide density<sup>2</sup>. Therefore, the modular design of this synthetic matrix allows the

study of the independent contributions of physicochemical matrix properties to IMCD cell tubulogenesis.

PEG-4MAL macromer was functionalized with adhesive peptide and crosslinked in the presence of IMCD cells to generate cell-encapsulating PEG-4MAL hydrogels (Supplementary Fig. 2a-c). These synthetic hydrogels were engineered to present a constant 2.0 mM RGD adhesive peptide (GRGDSPC) density and crosslinked with a synthetic peptide containing a protease degradable sequence found in type I collagen (GPQ-W: GCRDGPQGIWGQDRCG). The GPQ-W peptide is predominantly cleaved by MMP-1, -2 and -8<sup>23</sup>, and exhibits low reactivity for MT1-MMP<sup>24</sup>. The RGD adhesive peptide type and density and GPQ-W crosslinking peptide have been shown to support MDCK cell viability and cyst morphogenesis in PEG-4MAL hydrogels<sup>2</sup>. The mechanical properties of the hydrogel were tuned by varying polymer density (Supplementary Fig. 2d). Because ECM mechanical properties influence epithelial cell behaviors<sup>2,20</sup>, we investigated the influence of hydrogel polymer density (5-7% wt/vol; 10 kDa PEG-4MAL macromer) on IMCD cell viability and tubule formation (Fig. 1). This combination of macromer size and polymer densities can produce hydrogels with mechanical properties (storage modulus,  $G'$ : 500 Pa) that have been shown to support epithelial tubulogenesis<sup>21</sup>. After 14 d in culture, IMCD cell clusters showed high viability in all hydrogel conditions (Fig. 1a) and a polymer density-dependent effect on both projected area and longest distance between two points along the projected area (Feret diameter; Fig. 1b-d). At 21 d post-encapsulation, IMCD cell clusters maintained high viability in all hydrogel conditions (Fig. 1e), whilst no tubule formation or cell spreading was observed and size analysis demonstrated a polymer density-dependent effect on projected area and Feret diameter of the IMCD cell structures (Fig. 1f-h), demonstrating that these PEG-4MAL hydrogel formulations do not support tubulogenesis of IMCD cells.

Considering that proteolytic cleavage of ECM components by MT1-MMPs is essential for renal cell proliferation and tubulogenesis<sup>1,25</sup>, we then examined whether crosslinking of PEG-4MAL hydrogels with a MT1-MMP-sensitive crosslinking peptide supports IMCD cell tubulogenesis. IMCD cells were encapsulated in RGD-functionalized hydrogels of different polymer densities (5 – 8%, 10 kDa PEG-4MAL) and crosslinked with the MT1-MMP-sensitive crosslinking peptide IPES (GCRDIPESLRAGDRCG)<sup>23,24</sup>. These IPES-crosslinked hydrogels exhibited mechanical properties comparable to hydrogels of equal polymer densities but crosslinked with GPQ-W peptide (Supplementary Fig. 2d). IMCD cells embedded in IPES-crosslinked PEG-4MAL hydrogels maintained high viability at 1 d post-encapsulation in all

conditions (Fig. 2a,b). After 5 d in culture, IMCD cells generated cell clusters that showed significant polymer density-dependent effects on cell proliferation, projected area, and Feret diameter (Fig. 2c-f). When IMCD cell culture continued for at least 21 d, cell clusters within the 5% and 6% hydrogels developed tubules, as opposed to cells within 7% and 8% hydrogels which remained as round clusters (Fig. 2g). These results indicate that synthetic hydrogels crosslinked with the IPES peptide support IMCD tubulogenesis likely due to its specificity for MT1-MMP as compared to collagen-derived peptides (e.g. GPQ-W)<sup>23,24</sup>. Furthermore, polymer density has a significant effect on IMCD cell proliferation, multi-cellular growth, and tubule formation. Although 5% PEG-4MAL hydrogels supported tubule formation, this formulation was less likely to endure experimental handling compared to 6% PEG-4MAL hydrogels by 21 d in culture. We therefore selected 6.0% (10 kDa) PEG-MAL hydrogels crosslinked with the MT1-MMP-sensitive IPES crosslinker for subsequent studies.

#### *Adhesive peptide type directs tubule formation*

Cell adhesion receptor interactions with ECM components provide signals critical for cell survival, proliferation and tubulogenesis<sup>7,12,26-29</sup>. Therefore, we examined whether the adhesive peptide type in the synthetic hydrogel impacts IMCD tubule formation. IMCD cells were embedded within 6% PEG-4MAL (10 kDa) hydrogels crosslinked with a constant IPES density and functionalized with different cysteine-terminated adhesive peptides (all at 2.0 mM; Fig. 3): RGD, inactive scrambled peptide RDG (GRDGSPC), type I collagen-mimetic triple helical GFOGER (GYGGGP(GPP)<sub>5</sub>GFOGER(GPP)<sub>5</sub>GPC)<sup>30</sup>, and laminin  $\beta$ 1 chain-derived YIGSR (CGGEGYGEYIGSR)<sup>31</sup>. IMCD cells encapsulated in RGD-functionalized hydrogels exhibited the highest level of proliferation (Fig. 3a,b) and showed significant increases in projected area and Feret diameter as compared to GFOGER- or YIGSR-functionalized hydrogels at 5 d post-encapsulation (Fig. 3c,d). Additionally, IMCD cells encapsulated in PEG-4MAL hydrogels functionalized with inactive RDG peptide showed significant reductions in cell proliferation when compared to RGD (Fig. 3a,b) and smaller cluster size compared to other hydrogel conditions (Fig. 3c,d). Furthermore, at 21 d post-encapsulation, IMCD cell tubule formation was observed in the RGD and GFOGER gel formulations, whereas cells encapsulated in RDG or YIGSR-functionalized hydrogels did not generate tubules (Fig. 3e,f). These results show an adhesive peptide type-dependent effect on tubulogenesis of IMCD cells after 21 d in culture. We note that different synthetic peptides promote differences in cell responses within ECM-derived substrates<sup>32</sup>, which may ultimately contribute to the differences in cluster size and tubulogenesis observed among groups. For instance, fibronectin-derived peptides (e.g. RGD), in addition to increasing cell migration, augment integrin signaling<sup>33</sup> and

can induce expression of proteases, facilitating cell invasion<sup>34,35</sup>, and potentially influencing IMCD cluster size and tubulogenesis. As RGD-functionalized hydrogels supported the highest level of cell proliferation, and significant growth compared to other adhesive peptides, we used RGD-functionalized hydrogels for subsequent studies.

*PEG-4MAL macromer size promotes early tubulogenesis*

Because previous studies suggest that matrix elasticity influences epithelial cell behaviors<sup>2,20</sup>, we investigated the influence of a lower range of matrix elasticity on IMCD cell viability, proliferation, and tubule formation. As changes in PEG-4MAL macromer size and polymer density modulate hydrogel elasticity and permeability<sup>2,20</sup>, IMCD cells were encapsulated in hydrogels of 20 kDa macromer size and a range of polymer densities (8-14% wt/vol) that exhibit a lower range of matrix elasticity (Supplementary Fig. 2e) compared to 10 kDa PEG-4MAL hydrogels (Supplementary Fig. 2d). The synthetic hydrogels were functionalized with the adhesive peptide RGD and crosslinked using the MT1-MMP-sensitive IPES peptide. No differences in cell viability were observed in any of the hydrogel conditions at 1 d post-encapsulation (Fig. 4a,b), whereas IMCD cell proliferation, projected area and Feret diameter varied in a polymer density-dependent manner at 5 d post-encapsulation (Fig. 4c-f). Moreover, as early as 7 d after encapsulation, cell sprouting was observed in the 8% hydrogel whereas round cell clusters continued to develop in all other hydrogel formulations (Fig. 4g). By 14 d of culture in the synthetic matrix, tubule formation was observed in a polymer density-dependent manner, where the 8% PEG-4MAL hydrogel had a higher number of cell structures presenting tubules whereas significantly less tubule formation was observed in the higher (12% and 14%) polymer density conditions (Fig. 5a). IMCD cells formed multicellular structure phenotypes classified as: (1) “smooth clusters”, which are smooth-contoured, spherical-like aggregates, (2) “spiked clusters”, which are aggregates characteristically decorated by numerous thin cytoplasmic processes extending out radially from the bulk of the IMCD cluster into the surrounding matrix, in contrast to the smooth-contoured appearance of the “smooth clusters”, or (3) “tubules”, which are aggregates characteristically decorated by numerous cellular processes extending out into the surrounding matrix and forming a complex network of branching cords extending out from the initial processes, in accordance with previous reports<sup>21,36</sup> (Supplementary Fig. 3). Evaluation of the distribution of cell cluster morphologies showed a higher frequency of tubule formation in 8%, 20 kDa hydrogels compared to other hydrogel conditions (Fig. 5b). Further analysis of the Feret diameter of tubule-presenting cell structures demonstrated a significantly higher length of tubules in the 8%, 20 kDa PEG-4MAL hydrogels, as compared to tubules formed in 6%, 10 kDa hydrogels (Fig. 5c). These results



demonstrate that IMCD cell encapsulation in PEG-4MAL hydrogels of 20 kDa macromer size resulted in cell spreading and tubule formation at an earlier time point and with an increased length of tubules, when compared to IMCD tubules formed in synthetic hydrogels prepared with the 10 kDa macromer (Figs. 2, 4 and 5). The strong dependence of IMCD multicellular growth and tubulogenesis on hydrogel polymer density and macromer size suggests that tubule formation is regulated by hydrogel elasticity. However, changes in polymer density and macromer size also alter hydrogel permeability<sup>2</sup>. Although it is not possible to uncouple mechanical properties from diffusional properties over the range of polymer densities examined in this study, we have previously shown that viability, growth, and morphogenesis of different epithelial systems within RGD-functionalized PEG-4MAL hydrogels is independent from differences in permeability<sup>2,20</sup>. This result suggests that polymer density- or macromer size-dependent IMCD cell tubulogenesis is related to hydrogel mechanical properties; however, changes on IMCD tubulogenesis due to differences in permeability between PEG-4MAL macromers cannot be completely ruled out. Additional experiments revealed that, by 7 d post-encapsulation, cell viability was compromised in softer (6%, 20 kDa; Supplementary Fig. 4a) or in GPQ-W-crosslinked (8%, 20 kDa; Fig. Supplementary 4b) PEG-4MAL hydrogels, as compared to 8%, 20 kDa PEG-4MAL hydrogels (Supplementary Fig. 4c). Additionally, IMCD cells encapsulated in (8% 20 kDa) hydrogels crosslinked with a non-degradable molecule (hexa(ethylene glycol) dithiol, [PEGDT]) exhibited significantly lower viability and smaller cluster size (area and Feret diameter) at 3 d and 11 d post-encapsulation, respectively, as compared to IPES-crosslinked hydrogels (Supplementary Fig. 4d-g), showing that the survival and growth of IMCD structures are dependent on a degradable matrix. Therefore, we designated 8% 20 kDa PEG-4MAL crosslinked with IPES as the synthetic polymer density, macromer size and crosslinker that provides the physical support and biomechanical signals necessary for optimal IMCD cell growth and tubule formation within PEG-4MAL hydrogels.

#### *Adhesive peptide density in PEG-4MAL hydrogels regulates tubule formation*

We next examined the effects of RGD adhesive peptide density on tubulogenesis within PEG-4MAL hydrogels engineered to present optimal biochemical properties (8%, 20 kDa PEG-4MAL). A total density (2.0 mM) of a mixture of cell-adhesive RGD peptide and scrambled inactive RDG peptide was used to vary RGD density (0.4–2.0 mM) while maintaining identical structures among hydrogel formulations and constant IPES crosslinking peptide density (Fig. 6). Additionally, a hydrogel condition with a total RGD density of 4.0 mM (9.15%, 20 kDa) was used while preserving equal IPES crosslinking peptide density and

mechanical properties (Supplementary Fig. 2e, Fig. 6). Cell viability and proliferation at 1 and 5 d post-encapsulation, respectively, was insensitive to RGD peptide density (Fig. 6a-d). However, cluster area and Feret diameter showed a significant dependence on RGD density at 5 d post-encapsulation (Fig. 6e,f). Hydrogels presenting low ( $<2.0$  mM) RGD densities supported the formation of relatively small multicellular structures with no significant differences among the groups (0.4, 1.0 and 1.6 mM RGD; Fig. 6e,f). In contrast, hydrogels presenting high ( $\geq 2.0$  mM) RGD density formed larger structures with no statistical differences between these groups (2.0 and 4.0 mM RGD; Fig. 6e,f). Further analysis of cellular structures at 14 d post-encapsulation demonstrated a RGD density-dependent effect on the frequency and Feret diameter of tubule-presenting cell structures (Fig. 6g-i). No significant differences were observed between the high RGD density (2 and 4 mM) hydrogels. EdU staining of emerging tubules at 14 d post-encapsulation revealed that cell proliferation is not higher in emerging tubules than in the bulk of the multicellular cluster (Fig. 6j), suggesting that cell proliferation is not the only factor contributing to tubule formation. Together, these results are consistent with previous studies showing that adhesive ligand density regulates epithelial morphogenesis independent of cell proliferation<sup>2</sup>, and suggest that high RGD density may support formation of longer tubules within the synthetic hydrogels by promoting increased integrin-mediated cell migration and/or increased cell-cell contacts via  $\alpha$ -catenin activation. Given that differences in the level of cell proliferation exist among IMCD clusters within the same hydrogel condition, it is important to note that these observations are based on a population level and do not necessarily describe individual cell clusters. Taken together, these results identify an engineered hydrogel formulation (storage modulus,  $G'$ : 200 Pa; 8% polymer density; 20 kDa macromer size; 2.0 mM RGD adhesive peptide; IPES crosslinking peptide) that supports IMCD viability and optimized cell proliferation, growth and formation of tubules.

#### *Engineered hydrogel supports key features of IMCD cell tubule differentiation*

The IMCD cell tubulogenesis program is characterized by the 3D assembly of epithelial cells into tubules and formation of a differentiated epithelium<sup>1</sup>. Interactions between laminin and integrin receptors are required for renal epithelial differentiation<sup>1,3,7,37,38</sup>. Therefore, to further characterize IMCD tubule differentiation, we examined laminin secretion and the role of integrin receptors of IMCD cell tubules generated within the engineered synthetic matrix. Over 21 d in culture, the engineered synthetic hydrogel supported a substantial increase in the number of multicellular structures forming organized tubules over time (Supplementary Fig. 5a,b). Furthermore, the hydrogel-generated IMCD tubules demonstrated an organized tubular assembly with a lumen (Fig. 7a-c), and secretion of laminin into the basal side of the tubular



structures<sup>1,25</sup> (Fig. 7d,e). We next evaluated the role of integrin receptors and mediators of mechanotransduction pathways on IMCD cell tubulogenesis program within the engineered hydrogel. Previous studies have demonstrated that IMCD cell morphogenesis program requires sequential cell adhesion to ECM via laminin- ( $\alpha_3\beta_1$ ) and collagen- ( $\alpha_1\beta_1$  and  $\alpha_2\beta_1$ ) binding integrins that promote cell spreading, proliferation, and migration to ultimately form multicellular tubular structures<sup>1,7,38</sup>. Addition of blocking antibodies against  $\alpha_1$ ,  $\alpha_2$ , and  $\beta_1$  integrin subunits to IMCD culture resulted in significant reductions in tubule formation at 21 d post-encapsulation as compared to control group (DMSO; Supplementary Fig. 5c,d). Additionally, treatment with blebbistatin or Y-27632, which inhibit myosin II and Rho-associated kinase<sup>39,40</sup>, respectively, resulted in significant reductions in tubule formation (Supplementary Fig. 5c,d), indicating that cellular contractility is important to IMCD tubulogenesis.

Finally, as previous studies have shown that MT1-MMP proteolytic activity is required for renal epithelial branching tubulogenesis in biological matrices as early as 3 d post-encapsulation<sup>25,41</sup>, we further assessed MT1-MMP-mediated tubulogenesis of IMCD cells within engineered PEG-4MAL hydrogels. We incubated IMCD cells in a blocking antibody specific to the catalytic domain of MT1-MMP (AB6005) starting at 3 d post-encapsulation in the engineered hydrogel and demonstrated reduced tubule formation after 15 d of culture, compared with the vehicle-only (DMSO) control (Fig. 8a,b). Additionally, IMCD cell culture revealed an increased expression of MT1-MMP in the cell-hydrogel interface at the multicellular and single-cell level (Fig. 8c), suggesting that MT1-MMP acts at the cell surface to remodel the synthetic hydrogel matrix. Taken together, these results demonstrate that the engineered PEG-4MAL hydrogel robustly supports key features of tubular differentiation of IMCD cells. Additionally, these results provide preliminary indication that IMCD tubulogenesis in the synthetic matrix is also directed by cell receptor interactions with secreted laminin, cellular contractility, and MT1-MMP activity at initial stages of tubule development.

#### *PEG-4MAL hydrogel supports tubulogenesis of other kidney epithelial cells*

To determine whether the synthetic hydrogel can be used to study epithelial tubulogenesis of other kidney epithelial cells, murine renal proximal tubule cells (RPTC) were cultured in 6% and 10% 20 kDa PEG-4MAL hydrogels functionalized with 2.0 mM RGD adhesive peptide and crosslinked with IPES peptide. RPTC showed high viability in both conditions at 1 d post-encapsulation, with no significant differences between the groups (Supplementary Fig. 6a). After 28 d in culture, RPTC tubule formation was observed in the

10% hydrogel condition, whereas no tubule formation was observed in 6% hydrogels. Analysis of the Feret diameter of RPTC multicellular structures demonstrated formation of significantly larger structures in the 10% hydrogel as compared to 6% hydrogel (Supplementary Fig. 6b,c). These results establish PEG-4MAL hydrogels as a tunable platform that supports tubulogenesis of different kidney epithelial cell systems.

## Discussion

This research describes a fully-defined synthetic hydrogel with independent control over its proteolytic degradation, mechanical properties, and adhesive ligand type and density that serves as a modular platform to study the impact of biochemical and mechanical matrix properties on epithelial tubular morphogenesis. Systematic changes in hydrogel formulation to independently tune hydrogel macromer size and polymer density, adhesive ligand type and density, and MMP-dependent degradation revealed that each of these properties has profound effects on this coordinated multicellular morphogenetic process, including cell viability, proliferation, and tubular structure development. Additionally, we identified an engineered synthetic hydrogel formulation that promotes lumenized tubule formation, integrin- and MT1-MMP-mediated growth of tubules, and supports increases in the number and length of tubules over time. These new observations are not attainable when using biological ECMs due to experimental inability to decouple matrix biochemical and mechanical properties. Moreover, the mechanical properties and protease degradation characteristics that supported murine IMCD tubulogenesis in this study are different from those recently identified for human renal epithelial cells in heparin-based hydrogels<sup>21</sup>, and suggest differences between these two epithelial cell sources. This fully synthetic matrix addresses major limitations of biological materials or hydrogels associated with lot-to-lot compositional and structural variability and tumor-derived nature that severely restrict scale-up applications and clinical translation. Furthermore, the modular nature of this hydrogel platform allows the characterization of the elementary matrix property contributions to renal organ development.

## Methods

### Immunofluorescence analysis

Primary antibodies used were rabbit anti-laminin (L9393, Sigma), anti- $\beta$ -catenin (71-2700 ThermoFisher), and mouse anti-MT1-MMP (IM57, Millipore). Secondary antibodies used were goat anti-mouse IgG Alexa Fluor 647 (Thermo Fisher Scientific), mouse anti-rabbit IgG-

CFL 647 (sc-516251, Santa Cruz Biotechnology), and donkey anti-rabbit IgG Dylight 650 (84546, Thermo Fisher Scientific). Nuclei were stained with DAPI and actin was stained with rhodamine phalloidin (R415, Thermo Fisher Scientific). Antibody dilutions were performed according to manufacturer's recommendations. Gels were washed extensively in DPBS and fixed in 4% formaldehyde in DPBS for 20 min. Gels were incubated for 30 min in blocking buffer (1% bovine serum albumin, 1% goat serum, 0.1% fish skin gelatin, 0.5% Triton X-100, 0.05% sodium azide in PBS). Samples were incubated in primary antibodies diluted in blocking buffer at 4 °C overnight. Secondary antibodies, rhodamine phalloidin and nuclear stain (DAPI) were diluted in blocking buffer and incubated at 4 °C overnight. Fluorescent images for tubule assessment were captured with 20X, 40X, 60X and 100X objectives in a Nikon Eclipse Ti microscope connected to a C2+ confocal module. Area and Feret diameter of multicellular IMCD structures were measured from fluorescent images of specimen cross sections using ImageJ macros. Morphological scoring was performed by blinded researcher that was not involved in data acquisition. Relative fluorescence analysis was performed on z-stack fluorescent images stained for MT1-MMP using ImageJ macros.

### **Cell culture**

Immortalized mouse inner medullary collecting duct (IMCD) cells (isolated from  $\alpha$ v flox/flox mice, as described previously<sup>38,42</sup>) were maintained in Dulbecco's Modified Eagle's Medium (DMEM)/Nutrient Mixture F-12 Ham (DMEM/F-12 50/50; D8437, Sigma-Aldrich) supplemented with 10% fetal bovine serum (Life Technologies) and 1% antibiotic-antimycotic solution (MT-30-004-CI, MediaTech). Renal proximal tubule cells (RPTCs) (isolated from  $\beta$ 1 flox/flox mice, as described before<sup>43</sup>) were maintained in DMEM/F-12 50/50 (D8437, Sigma-Aldrich) supplemented with 2.5% fetal bovine serum (Life Technologies), 20 ng/mL hydrocortisone (H0135, Sigma), ITS media supplement (5  $\mu$ g/mL insulin - 5  $\mu$ g/mL transferrin - 5 ng/mL selenite; I1884, Sigma), 6.7 mg/mL 3,3',5-Triiodo-L-thyronine (T5516, Sigma), 0.096 mg/mL D-valine (V1255, Sigma), and 100  $\mu$ g/mL Normocin (ant-nr-2, InvivoGen). RPTCs were maintained at 33°C with 0.1% interferon gamma (14777, Sigma) in culture media during growth and expansion. At least 10 d before 3D encapsulation, RPTCs were cultured in absence of interferon gamma at 37°C to induce differentiation.

### **Hydrogel formation and 3D cell encapsulation**

PEG-4MAL hydrogels were prepared as described previously<sup>15</sup>. Briefly, PEG-4MAL macromer (MW 22,000 or 11,000; Laysan Bio) was dissolved in 4-(2-hydroxyethyl)piperazine-1-ethanesulfonic acid (HEPES) buffer (20 mM in DPBS, pH 7.4). Adhesive and crosslinking peptides were custom synthesized by AAPPTec. Adhesive peptides

RGD (GRGDSPC), GFOGER (GYGGGP(GPP)<sub>5</sub>GFOGER (GPP)<sub>5</sub>GPC), YIGSR (CGGEGYGEYIGSR) and RDG (GRDGSPC) were dissolved in HEPES at 10.0 mM (5X final ligand density) and mixed with PEG-4MAL at a 2:1 PEG-4MAL/ligand ratio to generate functionalized PEG-4MAL precursor. Bis-cysteine crosslinking peptides IPES (GCRDIPES↓LRAGDRCG; ↓ denotes enzymatic cleavage site) or GPQ-W (GCRDGPQG↓IWGQDRCG), or non-degradable crosslinking molecules hexa(ethylene glycol) dithiol (PEGDT, 734616; Sigma) was dissolved in HEPES at a density corresponding to 1:1 maleimide/cysteine ratio after accounting for maleimide groups reacted with adhesive peptide. Cells were resuspended at 5X final density in ice-cold serum-free media and kept on ice. To form hydrogels, adhesive peptide-functionalized PEG-4MAL macromer, cells, and crosslinking peptide were polymerized for 20 min before addition of complete growth medium. A final density of 75,000 cells/mL were encapsulated in all hydrogels. Matrigel<sup>TM</sup> encapsulation was performed as described previously<sup>9</sup>. Briefly, cells were resuspended in culture media at a density of 100,000 cells/mL and mixed with thawed Matrigel<sup>TM</sup> (354277, Corning) at a 1:1 Matrigel<sup>TM</sup>/cell mixture ratio. Full growth medium change was performed every 2 – 3 d for all experiments. Sample size was established as at least 4 gels per condition with the premise that an outcome present in 4 different gels under a specific condition will reveal the population behavior submitted to this given condition.

### Hydrogel characterization

The storage and loss moduli of hydrogels were assessed by dynamic oscillatory strain and frequency sweeps performed on a MCR 302 stress-controlled rheometer (Anton Paar) with a 9-mm diameter, 2° cone, and plate geometry. Oscillatory frequency sweeps were used to examine the storage and loss moduli ( $\omega = 0.5\text{--}100 \text{ rad s}^{-1}$ ) at a strain of 2.31%.

### Viability and proliferation assays

For cell viability assessment, PEG-4MAL gels were incubated in 0.5% collagenase I (Worthington Biochemical), 0.5  $\mu\text{M}$  C<sub>12</sub>-Resazurin (live; L34951, Thermo Fisher Scientific), and 1  $\mu\text{M}$  TOTO-3 iodide (dead; T3604, Thermo Fisher Scientific) in serum-free media until hydrogel was completely dissolved and cells settled at bottom of well. Proliferation was assayed using the Click-iT EdU Imaging Kit (C10338, Thermo Fisher Scientific) following manufacturer's instructions. EdU labeling was performed for 5.5 hr at a final concentration of 10  $\mu\text{M}$ . Samples were imaged with Nikon Plan Fluor 10 $\times$  (NA 0.30) or Plan Fluor 20 $\times$  (NA 0.45) objectives in a C2-Plus Confocal System (NIS Elements acquisition software). Cells were counted with ImageJ (NIH) macros.

### **Inhibition of mediators of mechanotransduction, MT1-MMP and integrin subunits**

Inhibition of myosin II or Rho-associated kinase was performed using blebbistatin (203389, Calbiochem) or Y-27632 (688002, Calbiochem), respectively, by adding 25  $\mu$ M to the growth medium 5 d after cell encapsulation in hydrogel. Inhibition of the MT1-MMP catalytic domain was performed by adding 2 or 6  $\mu$ g/mL of anti-MT1-MMP antibody (AB6005, Millipore) to the growth medium 3 d after cell encapsulation in hydrogel. Inhibition of integrin subunits  $\alpha$ 1,  $\alpha$ 2 or  $\beta$ 1 was performed by adding 0.5  $\mu$ g/mL of anti-rat/mouse CD49a (555001, BD Pharmingen), anti-rat/mouse CD49b (554998, BD Pharmingen) or AIIB2 (Developmental Studies Hybridoma Bank), respectively. Samples were imaged using a Nikon Eclipse Ti microscope connected to a C2+ confocal module.

### **Statistical analyses**

Statistical analyses were performed using GraphPad Prism 6.0. For normally distributed data with equal variances, one-way ANOVA with Tukey's multiple comparison test was used, and unpaired t-test with Welch's correction. For non-normally distributed data, Kruskal-Wallis with Dunn's multiple comparisons test was used. P-values of statistical significance are represented as \*\*\*\*P < 0.0001, \*\*\*P < 0.0002, \*\*P < 0.0021, \*P < 0.0332. A p-value < 0.05 was considered significant.

**Competing interests**

The authors declare no competing financial interests.

**Funding**

This research was supported by the NIH (R01 AR062368, R01 EB024322 to A.J.G and 5-T32-EB006343-10 for A.M.R.), the National Science Foundation Graduate Research Fellowship (DGE-1650044 to R.C.A.) and by the Alfred P. Sloan Foundation's Minority Ph.D. (MPHD) Program (G-2016-20166039 to R.C.A.).

**Author contributions**

R.C.A., A.M.R. and A.Y.C. conducted all experiments, collected data and performed data analyses. A.J.G., R.Z and R.C.A. conceptualized and designed the project and experiments. R.C.A., A.M.R., A.J.G. and R.Z. wrote the manuscript.

**Data availability**

All data supporting the findings of this study are available from the corresponding author on reasonable request.



## REFERENCES

- 1 Lelongt, B. & Ronco, P. Role of extracellular matrix in kidney development and repair. *Pediatric Nephrology* **18**, 731-742, doi:10.1007/s00467-003-1153-x (2003).
- 2 Enemchukwu, N. O. *et al.* Synthetic matrices reveal contributions of ECM biophysical and biochemical properties to epithelial morphogenesis. *The Journal of cell biology* **212**, 113-124, doi:10.1083/jcb.201506055 (2016).
- 3 Liu, Y. *et al.* Coordinate integrin and c-Met signaling regulate Wnt gene expression during epithelial morphogenesis. *Development (Cambridge, England)* **136**, 843-853, doi:10.1242/dev.027805 (2009).
- 4 Lucy Erin, O., Brien, Mirjam, M. P. Z. & Keith, E. M. Building epithelial architecture: insights from three-dimensional culture models. *Nature Reviews Molecular Cell Biology* **3**, 531, doi:10.1038/nrm859 (2002).
- 5 Lo, A., Mori, H., Mott, J. & Bissell, M. Constructing Three-Dimensional Models to Study Mammary Gland Branching Morphogenesis and Functional Differentiation. *Journal Of Mammary Gland Biology And Neoplasia* **17**, 103-110, doi:10.1007/s10911-012-9251-7 (2012).
- 6 Sakurai, H., Barros, E., Tsukamoto, T., Barasch, J. & Nigam, S. An in vitro tubulogenesis system using cell lines derived from the embryonic kidney shows dependence on multiple soluble growth factors. *Proceedings of the National Academy of Sciences, USA* **94**, 6279-6284 (1997).
- 7 Chen, D. *et al.* Differential expression of collagen- and laminin-binding integrins mediates ureteric bud and inner medullary collecting duct cell tubulogenesis. *American Journal of Physiology-Renal Physiology* **287**, F602-F611, doi:10.1152/ajprenal.00015.2004 (2004).
- 8 Rosines, E. *et al.* Constructing kidney-like tissues from cells based on programs for organ development: toward a method of in vitro tissue engineering of the kidney. *Tissue engineering. Part A* **16**, 2441-2455, doi:10.1089/ten.TEA.2009.0548 (2010).
- 9 Giles, R. H., Ajzenberg, H. & Jackson, P. K. 3D spheroid model of mIMCD3 cells for studying ciliopathies and renal epithelial disorders. *Nature Protocols* **9**, 2725, doi:10.1038/nprot.2014.181  
<https://www.nature.com/articles/nprot.2014.181#supplementary-information> (2014).
- 10 Yu, W. *et al.*  $\beta$ 1-Integrin Orients Epithelial Polarity via Rac1 and Laminin. *Molecular Biology of the Cell* **16**, 433-445, doi:10.1091/mbc.E04-05-0435 (2005).
- 11 Hughes, C. S., Postovit, L. M. & Lajoie, G. A. Matrigel: a complex protein mixture required for optimal growth of cell culture. *Proteomics* **10**, 1886-1890, doi:10.1002/pmic.200900758 (2010).

- 12 Cruz-Acuña, R. & García, A. J. Synthetic hydrogels mimicking basement membrane matrices to promote cell-matrix interactions. *Matrix Biology*, doi:<http://dx.doi.org/10.1016/j.matbio.2016.06.002> (2016).
- 13 Gjorevski, N., Ranga, A. & Lutolf, M. P. Bioengineering approaches to guide stem cell-based organogenesis. *Development* **141**, 1794-1804, doi:10.1242/dev.101048 (2014).
- 14 Gjorevski, N. *et al.* Designer matrices for intestinal stem cell and organoid culture. *Nature* **539**, 560-564, doi:10.1038/nature20168 (2016).
- 15 Cruz-Acuña, R. *et al.* PEG-4MAL hydrogels for human organoid generation, culture, and in vivo delivery. *Nature Protocols*, doi:10.1038/s41596-018-0036-3 (2018).
- 16 Caliri, S. R. & Burdick, J. A. A practical guide to hydrogels for cell culture. *Nature methods* **13**, 405-414, doi:10.1038/nmeth.3839 (2016).
- 17 Kloxin, A. M., Kasko, A. M., Salinas, C. N. & Anseth, K. S. Photodegradable hydrogels for dynamic tuning of physical and chemical properties. *Science (New York, N.Y.)* **324**, 59-63, doi:10.1126/science.1169494 (2009).
- 18 Lutolf, M. P. & Hubbell, J. A. Synthetic biomaterials as instructive extracellular microenvironments for morphogenesis in tissue engineering. *Nature Biotechnology* **23**, 47+, doi:10.1038/nbt1055 (2005).
- 19 Madl, C. M., Heilshorn, S. C. & Blau, H. M. Bioengineering strategies to accelerate stem cell therapeutics. *Nature* **557**, 335-342, doi:10.1038/s41586-018-0089-z (2018).
- 20 Cruz-Acuña, R. *et al.* Synthetic hydrogels for human intestinal organoid generation and colonic wound repair. *Nature cell biology*, doi:10.1038/ncb3632 (2017).
- 21 Weber, H. M., Tsurkan, M. V., Magno, V., Freudenberg, U. & Werner, C. Heparin-based hydrogels induce human renal tubulogenesis in vitro. *Acta Biomaterialia* **57**, 59-69, doi:<https://doi.org/10.1016/j.actbio.2017.05.035> (2017).
- 22 Phelps, E. A. *et al.* Maleimide cross-linked bioactive PEG hydrogel exhibits improved reaction kinetics and cross-linking for cell encapsulation and in situ delivery. *Advanced materials* **24**, 64-70, 62, doi:10.1002/adma.201103574 (2012).
- 23 Patterson, J. & Hubbell, J. A. Enhanced proteolytic degradation of molecularly engineered PEG hydrogels in response to MMP-1 and MMP-2. *Biomaterials* **31**, 7836-7845, doi:<https://doi.org/10.1016/j.biomaterials.2010.06.061> (2010).
- 24 Turk, B. E., Huang, L. L., Piro, E. T. & Cantley, L. C. Determination of protease cleavage site motifs using mixture-based oriented peptide libraries. *Nature Biotechnology* **19**, 661, doi:10.1038/90273 (2001).
- 25 Riggins, K. S. *et al.* MT1-MMP-mediated basement membrane remodeling modulates renal development. *Experimental Cell Research* **316**, 2993-3005, doi:<https://doi.org/10.1016/j.yexcr.2010.08.003> (2010).

- 26 Wickström, S. A., Radovanac, K. & Fässler, R. Genetic Analyses of Integrin Signaling. *Cold Spring Harbor Perspectives in Biology* **3**, a005116, doi:10.1101/cshperspect.a005116 (2011).
- 27 Hynes, R. O. Integrins: Bidirectional, Allosteric Signaling Machines. *Cell* **110**, 673-687, doi:https://doi.org/10.1016/S0092-8674(02)00971-6 (2002).
- 28 Giancotti, F. G. & Ruoslahti, E. Integrin Signaling. *Science* **285**, 1028, doi:10.1126/science.285.5430.1028 (1999).
- 29 Adams, J. C. & Watt, F. M. Regulation of development and differentiation by the extracellular matrix. *Development* **117**, 1183, PMID: 8404525 (1993).
- 30 Emsley, J., Knight, C. G., Farndale, R. W. & Barnes, M. J. Structure of the Integrin  $\alpha 2\beta 1$ -binding Collagen Peptide. *Journal of Molecular Biology* **335**, 1019-1028, doi:10.1016/j.jmb.2003.11.030 (2004).
- 31 Kikkawa, Y. *et al.* Laminin-111-derived peptides and cancer. *Cell adhesion & migration* **7**, 150-256, doi:10.4161/cam.22827 (2013).
- 32 Livant, D. L. *et al.* The PHSRN sequence induces extracellular matrix invasion and accelerates wound healing in obese diabetic mice. *The Journal of clinical investigation* **105**, 1537-1545, doi:10.1172/JCI8527 (2000).
- 33 Miyamoto, S., Akiyama, S. K. & Yamada, K. M. Synergistic roles for receptor occupancy and aggregation in integrin transmembrane function. *Science* **267**, 883, doi:10.1126/science.7846531 (1995).
- 34 Werb, Z., Tremble, P. M., Behrendtsen, O., Crowley, E. & Damsky, C. H. Signal transduction through the fibronectin receptor induces collagenase and stromelysin gene expression. *The Journal of cell biology* **109**, 877, doi:10.1083/jcb.109.2.877 (1989).
- 35 Lash, J. W., Linask, K. K. & Yamada, K. M. Synthetic peptides that mimic the adhesive recognition signal of fibronectin: Differential effects on cell-cell and cell-substratum adhesion in embryonic chick cells. *Developmental Biology* **123**, 411-420, doi:https://doi.org/10.1016/0012-1606(87)90399-X (1987).
- 36 Montesano, R., Schaller, G. & Orci, L. Induction of epithelial tubular morphogenesis in vitro by fibroblast-derived soluble factors. *Cell* **66**, 697-711, doi:10.1016/0092-8674(91)90115-F.
- 37 Zent, R. *et al.* Involvement of Laminin Binding Integrins and Laminin-5 in Branching Morphogenesis of the Ureteric Bud during Kidney Development. *Developmental Biology* **238**, 289-302, doi:https://doi.org/10.1006/dbio.2001.0391 (2001).
- 38 Zhang, X. *et al.*  $\beta 1$  integrin is necessary for ureteric bud branching morphogenesis and maintenance of collecting duct structural integrity. *Development* **136**, 3357, doi:10.1242/dev.036269 (2009).
- 39 Straight, A. F. *et al.* Dissecting Temporal and Spatial Control of Cytokinesis with a Myosin II Inhibitor. *Science* **299**, 1743-1747, doi: 10.1126/science.1081412 (2003).

- 40 Uehata, M. *et al.* Calcium sensitization of smooth muscle mediated by a Rho-associated protein kinase in hypertension. *Nature* **389**, 990-994, doi: 10.1038/40187 (1997).
- 41 Pohl, M., Sakurai, H., Bush, K. T. & Nigam, S. K. Matrix metalloproteinases and their inhibitors regulate in vitro ureteric bud branching morphogenesis. *American Journal of Physiology-Renal Physiology* **279**, F891-F900, doi:10.1152/ajprenal.2000.279.5.F891 (2000).
- 42 Husted, R. F., Hayashi, M. & Stokes, J. B. Characteristics of papillary collecting duct cells in primary culture. *American Journal of Physiology-Renal Physiology* **255**, F1160-F1169, doi:10.1152/ajprenal.1988.255.6.F1160 (1988).
- 43 Elias, B. C. *et al.* The integrin  $\beta 1$  subunit regulates paracellular permeability of kidney proximal tubule cells. *J Biol Chem* **289**, 8532-8544, doi:10.1074/jbc.M113.526509 (2014).

## Figures

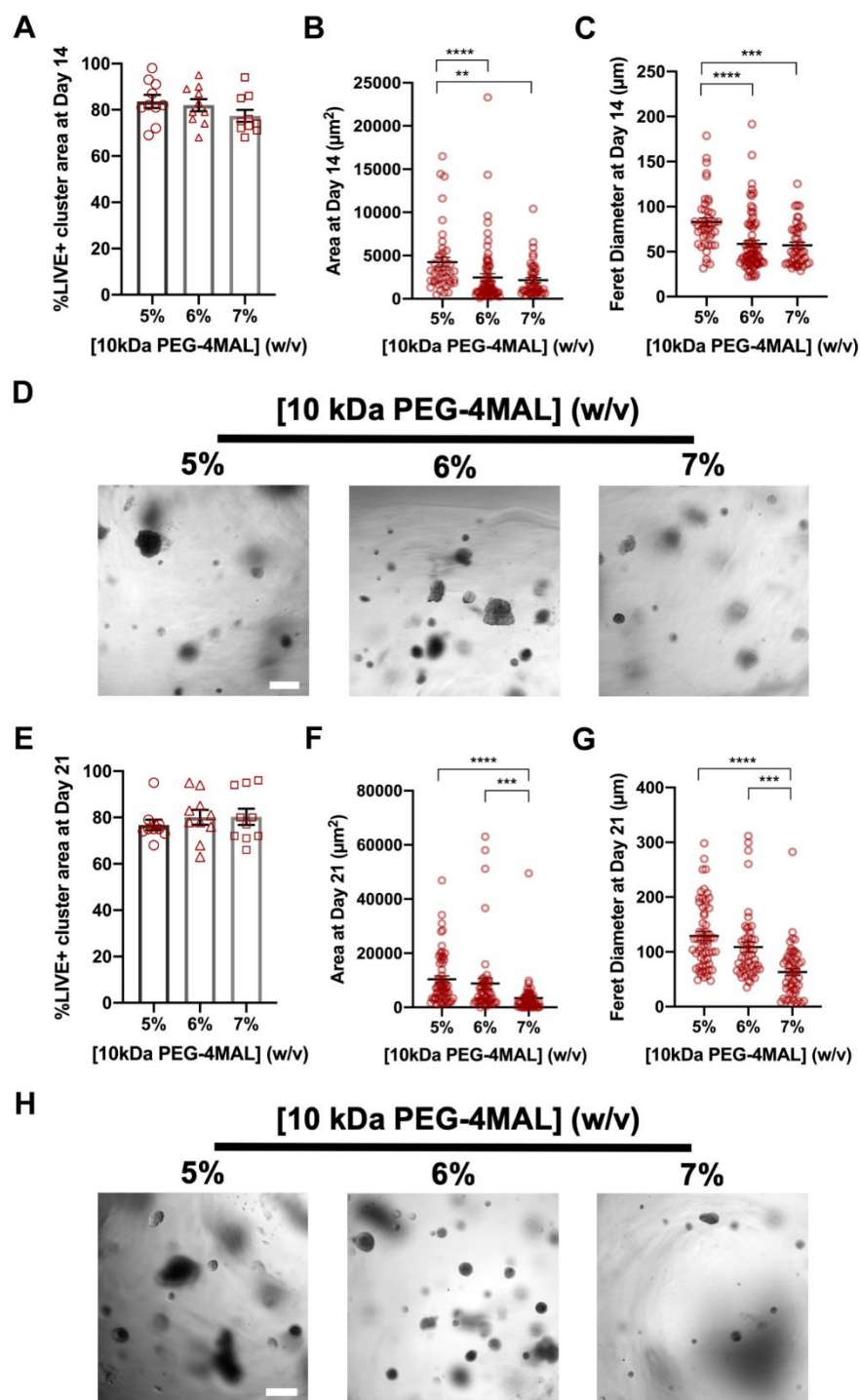


**Figure 1: PEG-4MAL hydrogel crosslinked with GPQ-W peptide does not support tubule formation.** (a) Percentage of IMCD cluster area that stained for LIVE (C<sub>12</sub>-Resazurin) after 14 d of encapsulation in PEG-4MAL hydrogels of different polymer density and crosslinked with GPQ-W peptide (mean  $\pm$  SEM). IMCD multicellular structure (b) projected area and (c) Feret diameter at 14 d after encapsulation in PEG-4MAL hydrogel. (d) Transmitted light images of IMCD cells cultured in PEG-4MAL hydrogels. Bar, 100  $\mu$ m. (e) Percentage of IMCD cluster area that stained for LIVE (C<sub>12</sub>-Resazurin) after 21 d of encapsulation in PEG-4MAL hydrogels (mean  $\pm$  SEM). IMCD multicellular structure (f) projected area and (g) Feret diameter at 21 d after encapsulation in PEG-4MAL hydrogels. (h) Transmitted light images of IMCD cells at 21 d after encapsulation in PEG-4MAL hydrogels. Bar, 200  $\mu$ m. Graph lines represents the mean of the individual data points. Each data point represents one multicellular structure. Kruskal-Wallis with Dunn's multiple comparisons test was used. P-values of statistical significance are represented as \*\*\*\*P < 0.0001, \*\*\*P < 0.0002, \*\*P < 0.0021. An adjusted p-value < 0.05 was considered significant. Experiments performed with 6 PEG-4MAL hydrogels per experimental group. Four independent experiments were performed and data are presented for one of the experiments.



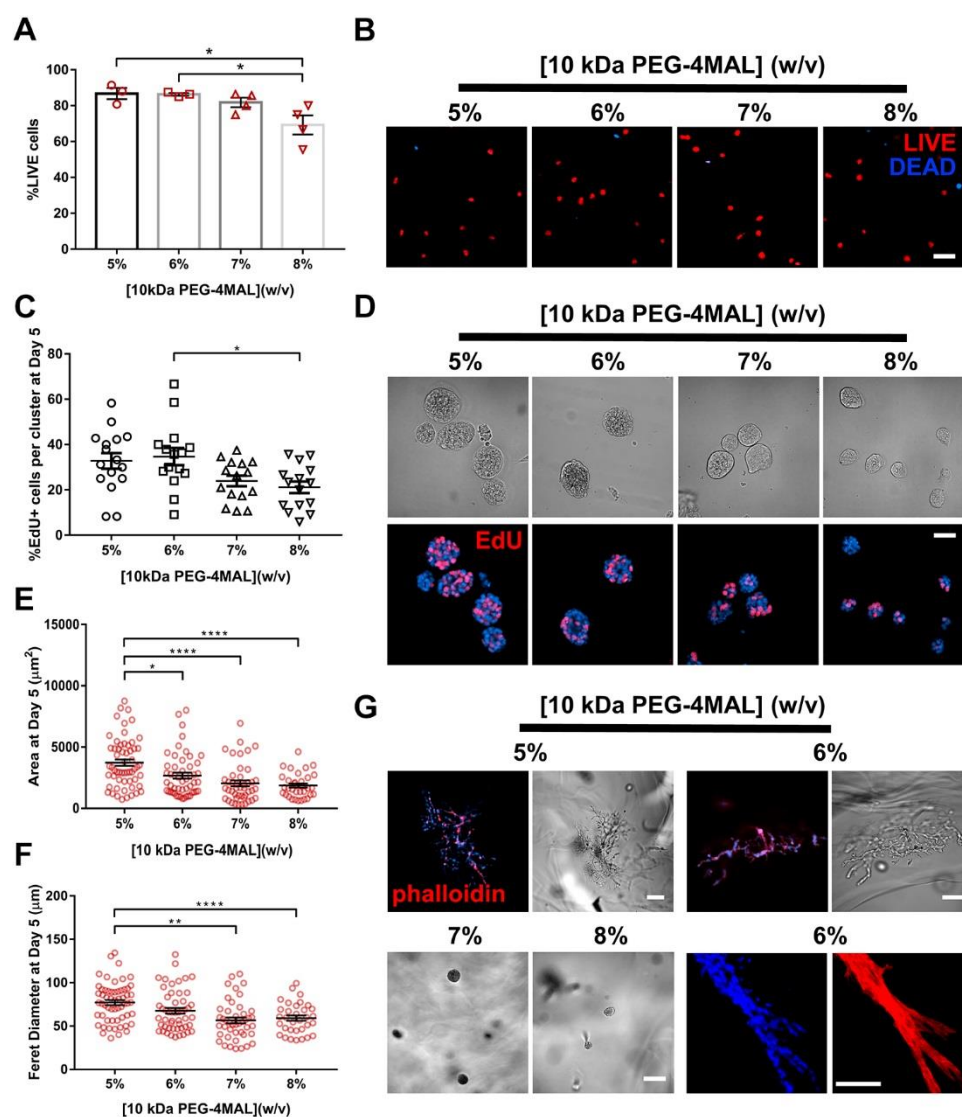


**Figure 2: Polymer density of 10 kDa PEG-4MAL directs tubule formation.** (a) Percentage of IMCD cells that stained for LIVE (C<sub>12</sub>-Resazurin) after 1 d of encapsulation in 10 kDa PEG-4MAL hydrogels of different polymer density (mean  $\pm$  SEM). Each data point represents one hydrogel sample. At least 100 cells were assessed per condition. (b) Fluorescence microscopy images of IMCD cells cultured in PEG-4MAL hydrogels of different polymer density. IMCD cell viability was assessed at 1 d after encapsulation. Bar, 100  $\mu$ m. (c) Percentage of IMCD cells per cluster that were labeled by EdU incorporation (mean  $\pm$  SEM) after 5 d of encapsulation. At least 30 clusters were analyzed per condition. (d) Transmitted light and fluorescence microscopy images of proliferating (EdU+) IMCD cells cultured in PEG-4MAL

hydrogels of different polymer density. IMCD cell proliferation was assessed at 5 d after encapsulation. Bar, 50  $\mu\text{m}$ . IMCD multicellular structure (e) projected area and (f) Feret diameter at 5 d after encapsulation in PEG-4MAL hydrogel. Graph line represents the mean of the individual data points. Each data point represents one multicellular structure. (g) Transmitted light and fluorescence microscopy images of IMCD cells at 21 d after encapsulation in PEG-4MAL hydrogel and labeled for actin (phalloidin). DAPI, counterstain. Bars, 100  $\mu\text{m}$ . Kruskal-Wallis with Dunn's multiple comparisons test was used. P-values of statistical significance are represented as \*\*\*\*P < 0.0001, \*\*\*P < 0.0002, \*P < 0.0332. An adjusted p-value < 0.05 was considered significant. Experiments performed with 6 PEG-4MAL hydrogels per experimental group. Three independent experiments were performed and data are presented for one of the experiments.

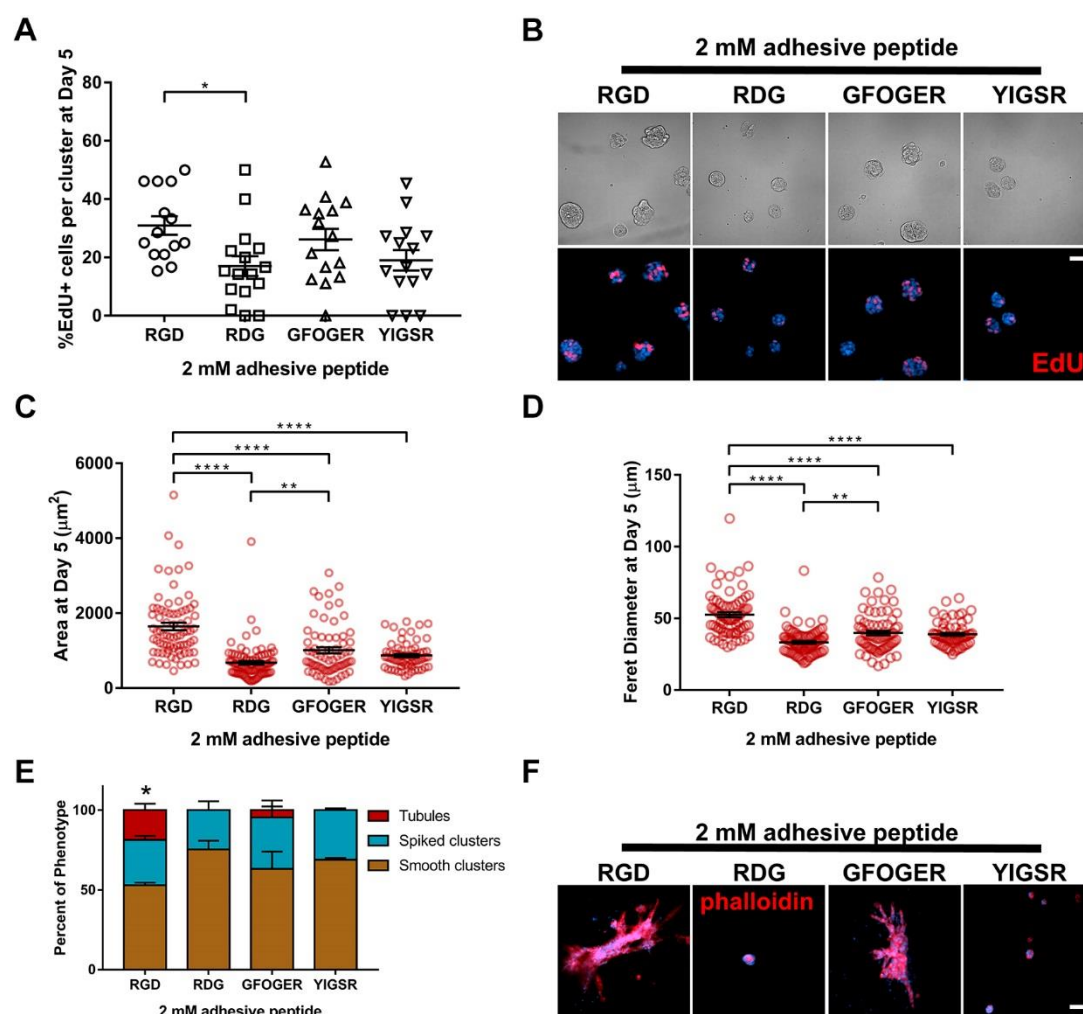


**Figure 3: Adhesive peptide type in PEG-4MAL hydrogels directs tubule formation.** (a) Percentage of IMCD cells per cluster that were labeled by EdU incorporation (mean  $\pm$  SEM) after 5 d of encapsulation in PEG-4MAL hydrogels functionalized with different adhesive peptides. At least 30 clusters were analyzed per condition. (b) Transmitted light and fluorescence microscopy images of proliferating (EdU+) IMCD cells cultured in PEG-4MAL hydrogels functionalized with different adhesive peptides. IMCD cell proliferation was assessed at 5 d after encapsulation. Bar, 50  $\mu\text{m}$ . IMCD multicellular structure (c) projected area and (d) Feret diameter at 5 d after encapsulation in PEG-4MAL hydrogel. Graph line represents the mean of the individual data points. Each data point represents one multicellular structure. (e) Percentage of IMCD multicellular structures (mean  $\pm$  SEM) that classified as either “smooth

clusters”, “spiked clusters”, or “tubules” after 21 d of encapsulation. At least 10 multicellular structures were analyzed per condition. (f) Fluorescence microscopy images of IMCD cells at 21 d after encapsulation in PEG-4MAL hydrogel and labeled for actin (phalloidin). DAPI, counterstain. Bars, 50  $\mu$ m. (a,c,d) Kruskal-Wallis with Dunn’s multiple comparisons test was used. (e)  $\chi^2$  test with Bonferroni’s correction was used; \*,  $P < 0.0002$  for RGD vs RDG and  $P < 0.0021$  for RGD vs YIGSR. P-values of statistical significance are represented as \*\*\*\* $P < 0.0001$ , \*\* $P < 0.0021$ , \* $P < 0.0332$ . An adjusted p-value  $< 0.05$  was considered significant. Experiments performed with 6 PEG-4MAL hydrogels per experimental group. Three independent experiments were performed and data are presented for one of the experiments.

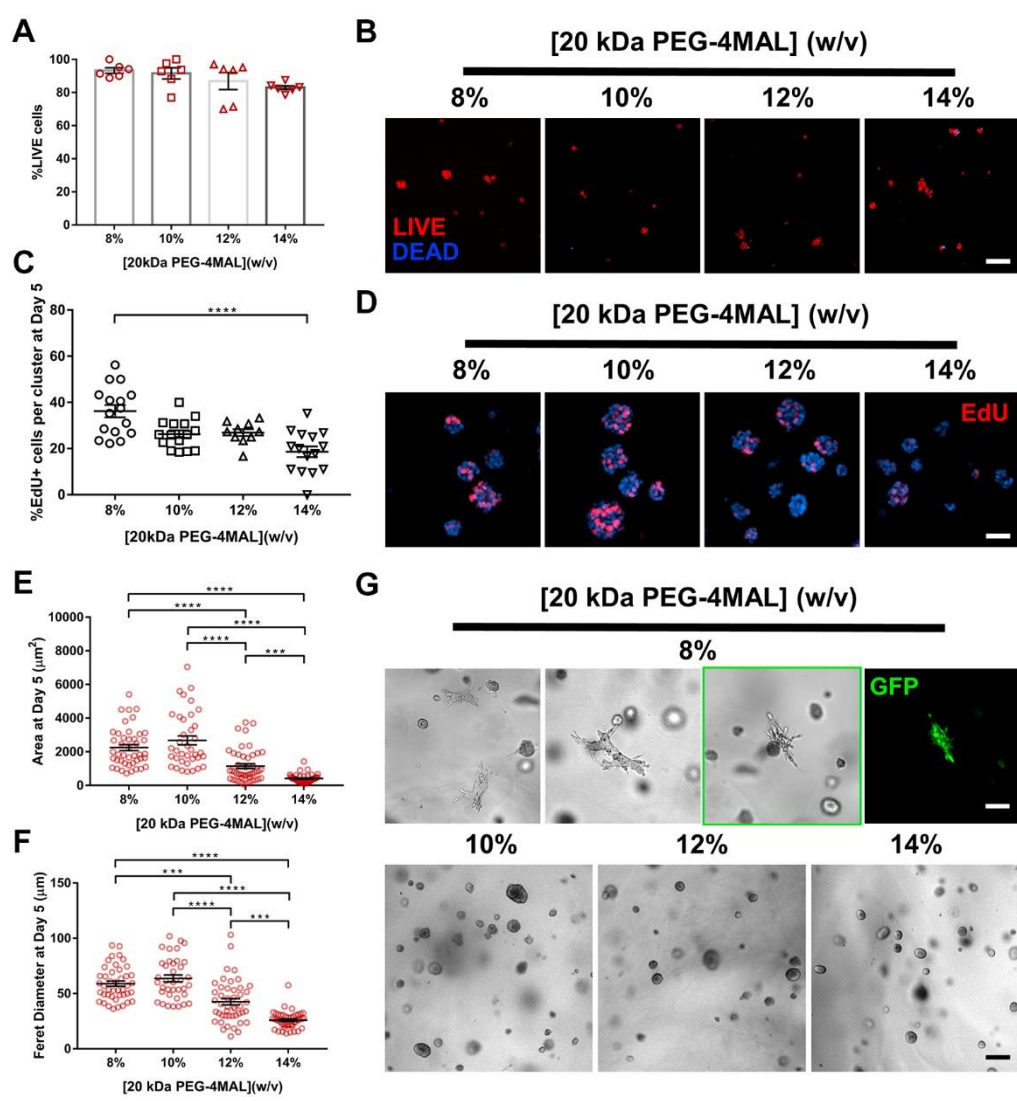


**Figure 4: Polymer density of 20 kDa PEG-4MAL directs tubule formation.** (a) Percentage of IMCD cells that stained for LIVE (C<sub>12</sub>-Resazurin) after 1 d of encapsulation in 20 kDa PEG-4MAL hydrogels of different polymer density (mean ± SEM). Each data point represents one independent hydrogel. At least 100 cells were assessed per condition. (b) Fluorescence microscopy images of IMCD cells cultured in PEG-4MAL hydrogels of different polymer density. IMCD cell viability was assessed at 1 d after encapsulation. Bar, 50 μm. (c) Percentage of IMCD cells per cluster that were labeled by EdU incorporation (mean ± SEM) after 5 d of encapsulation. At least 30 clusters were analyzed per condition. (d) Fluorescence microscopy images of proliferating (EdU+) IMCD cells cultured in PEG-4MAL hydrogels of different

polymer density. IMCD cell proliferation was assessed at 5 d after encapsulation. Bar, 50  $\mu\text{m}$ . IMCD multicellular structure (e) projected area and (f) Feret diameter at 5 d after encapsulation in PEG-4MAL hydrogel. Graph line represents the mean of the individual data points. Each data point represents one multicellular structure. (g) Transmitted light and fluorescence microscopy images of IMCD cells at 7 d after encapsulation in PEG-4MAL hydrogel. Bars, 100  $\mu\text{m}$  for 8% and 200  $\mu\text{m}$  for other conditions. Kruskal-Wallis with Dunn's multiple comparisons test was used. P-values of statistical significance are represented as \*\*\*\*P < 0.0001, \*\*\*P < 0.0002. An adjusted p-value < 0.05 was considered significant. Experiments performed with 6 PEG-4MAL hydrogels per experimental group. Three independent experiments were performed and data are presented for one of the experiments.



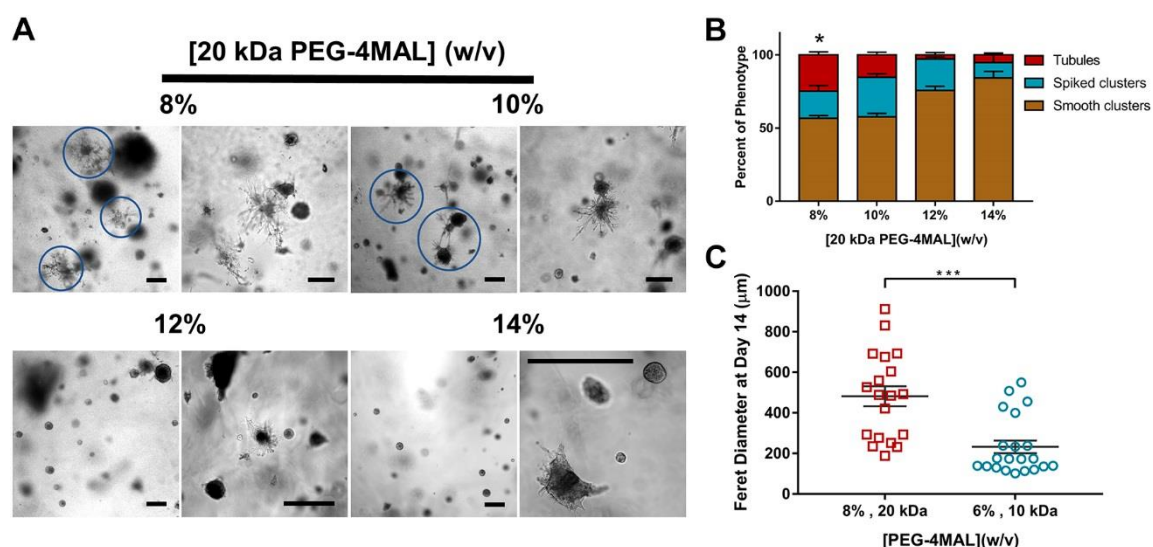


**Figure 5: Polymer density and macromer size controls tubule formation.** (a) Transmitted light images of IMCD cells cultured in 20 kDa PEG-4MAL hydrogels of different polymer density at 14 d after encapsulation. Bar, 200  $\mu\text{m}$ . (b) Percentage of IMCD multicellular structures (mean  $\pm$  SEM) that classified as either “smooth clusters”, “spiked clusters”, or “tubules” after 21 d of encapsulation. At least 10 multicellular structures were analyzed per condition.  $\chi^2$  test with Bonferroni’s correction was used; \*,  $P < 0.0001$  for 8% vs 12% and  $P < 0.0002$  for 8% vs 14%. (c) IMCD multicellular structure Feret diameter at 14 d after encapsulation in PEG-4MAL hydrogels of different macromer size. Graph line represents the mean of the individual data points. Each data point represents one multicellular structure. Unpaired t-test with Welch’s correction was used. P-value of statistical significance is represented as \*\*\* $P < 0.0002$ . An adjusted p-value  $< 0.05$  was considered significant. Experiments performed with 6 PEG-4MAL hydrogels per experimental group. Three independent experiments were performed and data are presented for one of the experiments.

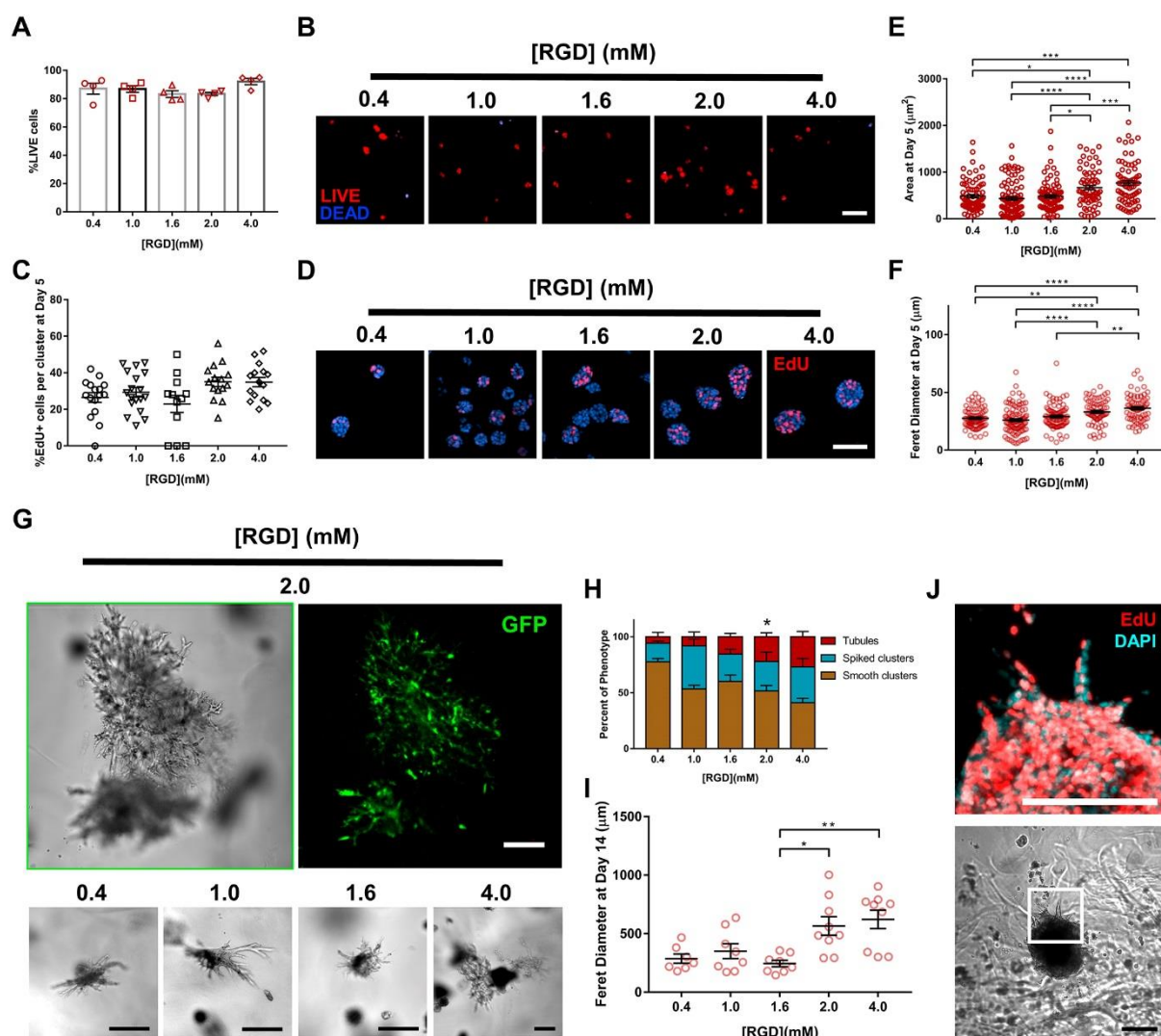


**Figure 6: Adhesive peptide density in PEG-4MAL hydrogels regulates tubule formation.**

(a) Percentage of IMCD cells that stained for LIVE (C<sub>12</sub>-Resazurin) after 1 d of encapsulation in 8%, 20 kDa PEG-4MAL hydrogels functionalized with varying RGD density and crosslinked with IPES peptide (mean  $\pm$  SEM). Each data point represents one independent hydrogel. At least 100 cells were assessed per condition. (b) Fluorescence microscopy images of IMCD cells cultured in PEG-4MAL hydrogel. IMCD cell viability was assessed at 1 d after encapsulation. Bar, 50  $\mu$ m. (c) Percentage of IMCD cells per cluster that were labeled by EdU incorporation (mean  $\pm$  SEM) after 5 d of encapsulation. At least 30 clusters were analyzed per condition. (d) Fluorescence microscopy images of proliferating (EdU+) IMCD cells cultured

in PEG-4MAL hydrogels of different polymer density. IMCD cell proliferation was assessed at 5 d after encapsulation. Bar, 50  $\mu\text{m}$ . IMCD multicellular structure (e) projected area and (f) Feret diameter at 5 d after encapsulation in PEG-4MAL hydrogel. Graph line represents the mean of the individual data points. Each data point represents one multicellular structure. (g) Transmitted light and fluorescence microscopy images of GFP-expressing IMCD cells at 14 d after encapsulation in PEG-4MAL hydrogel. Bars, 100  $\mu\text{m}$ . (h) Percentage of IMCD multicellular structures (mean  $\pm$  SEM) that classified as “smooth clusters”, “spiked clusters”, or “tubules” after 14 d of encapsulation. At least 10 multicellular structures were analyzed per condition.  $\chi^2$  test with Bonferroni’s correction was used; \*,  $P < 0.0021$  for 2.0 vs 0.4 mM RGD. (i) IMCD multicellular structure Feret diameter at 14 d after encapsulation in PEG-4MAL hydrogel. Graph line represents the mean of the individual data points. Each data point represents one multicellular structure. Kruskal-Wallis with Dunn’s multiple comparisons test was used. P-values of statistical significance are represented as \*\*\*\* $P < 0.0001$ , \*\*\* $P < 0.0002$ , \*\* $P < 0.0021$ , \* $P < 0.0332$ . An adjusted p-value  $< 0.05$  was considered significant. (j) Transmitted light and fluorescence microscopy images of proliferating (EdU+) IMCD cells cultured in PEG-4MAL hydrogels functionalized with 2.0 mM RGD. Bars, 100  $\mu\text{m}$ . Experiments performed with 6 PEG-4MAL hydrogels per experimental group. Three independent experiments were performed and data are presented for one of the experiments.

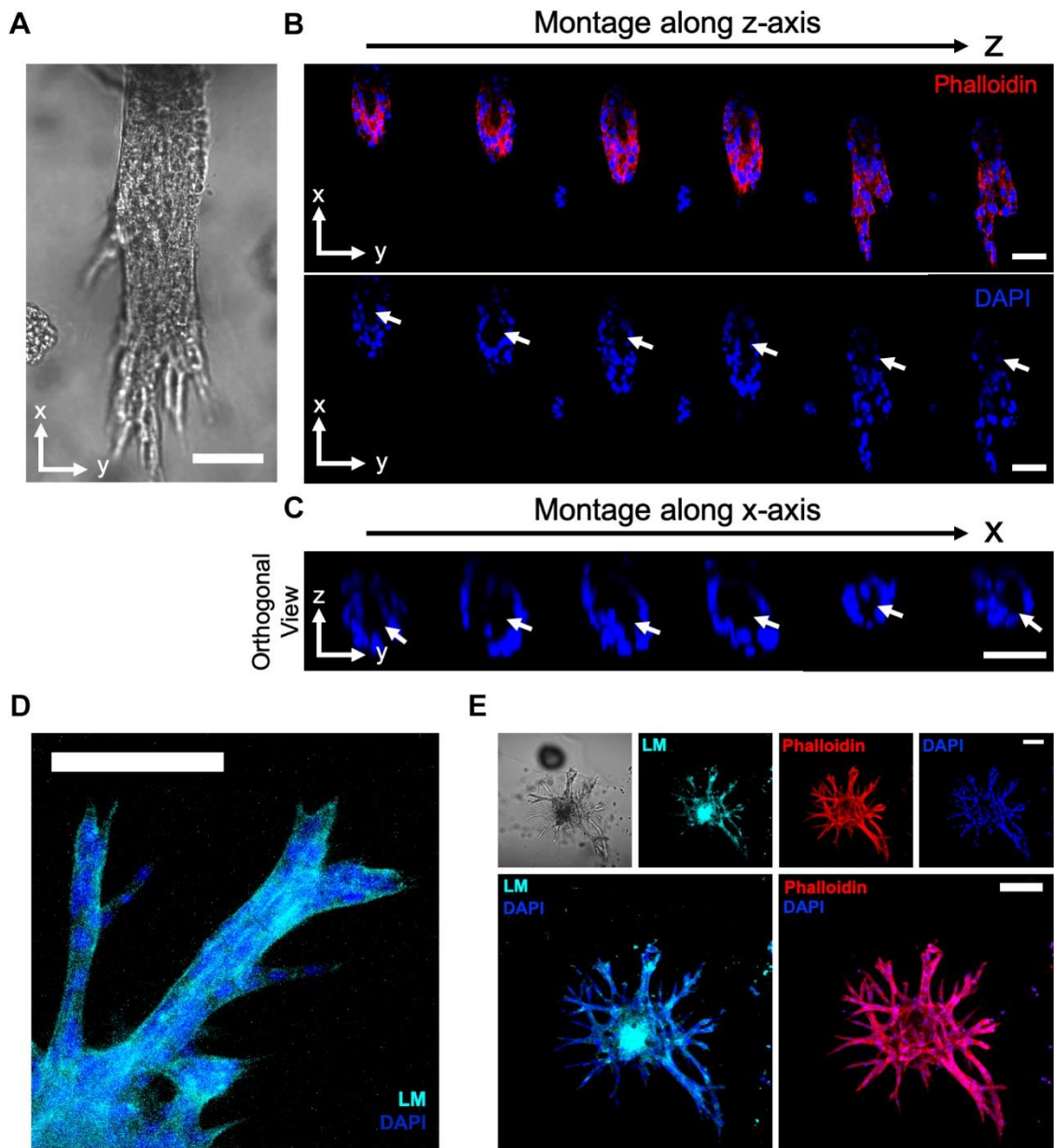


**Figure 7: Engineered PEG-4MAL hydrogel promotes key features of epithelial tubule differentiation.** (a-c) Transmitted light and fluorescence microscopy images of a lumenized IMCD tubule within engineered hydrogel stained for actin (phalloidin) and nuclei (DAPI). White arrows show lumen. Bars, 50  $\mu\text{m}$ . (d) Fluorescence microscopy image of IMCD tubules within engineered hydrogel stained for secreted laminin (LM). Bars, 100  $\mu\text{m}$ . (e) Transmitted light and fluorescence microscopy images of IMCD tubules within engineered hydrogel stained

for LM, actin (phalloidin) and nuclei (DAPI). Bars, 100  $\mu\text{m}$ . Experiments performed with 6 PEG-4MAL hydrogels per experimental group. Three independent experiments were performed and data are presented for one of the experiments.



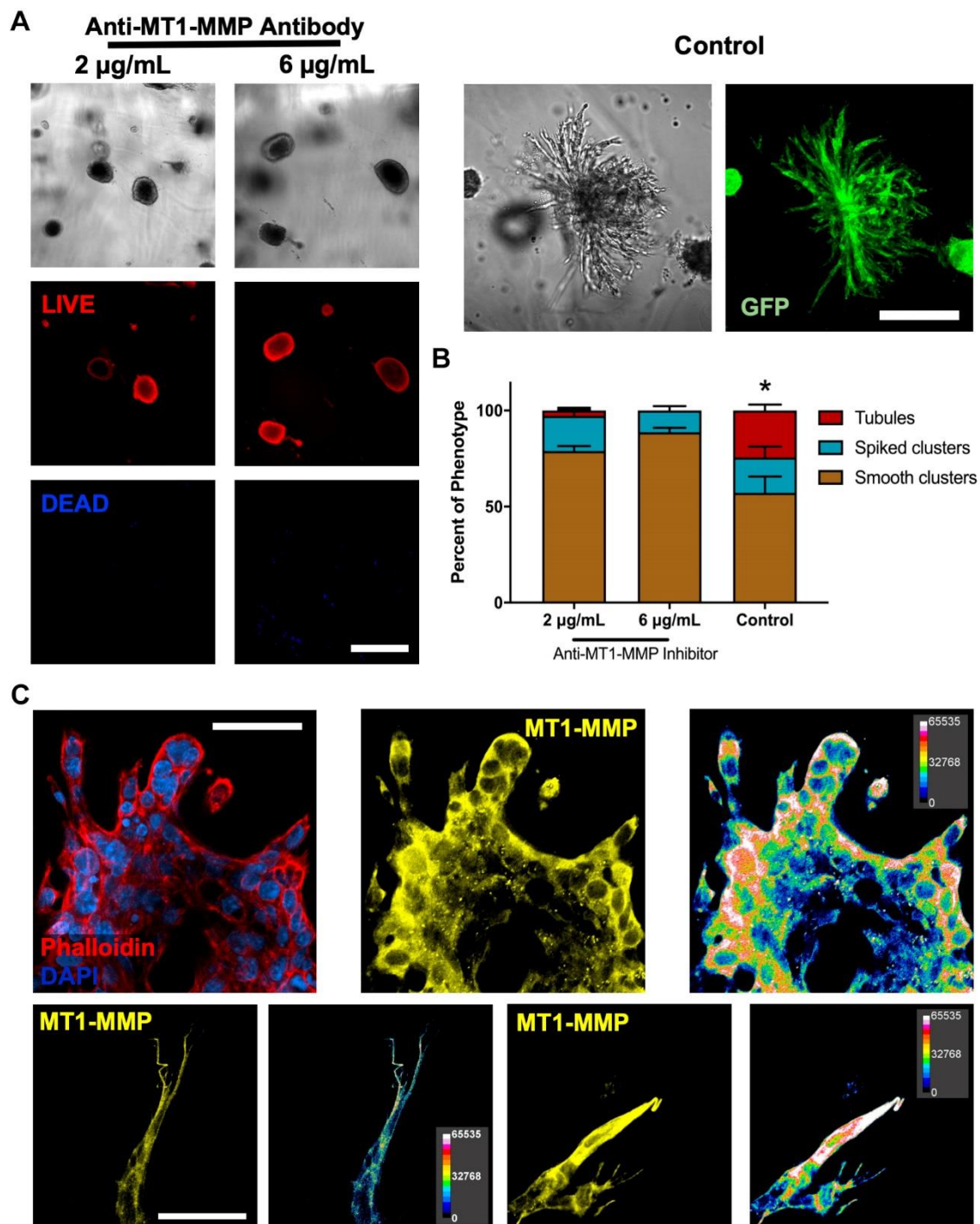


**Figure 8: PEG-4MAL hydrogels supports MMP-mediated tubule formation.** (a) Transmitted light and fluorescence microscopy images of IMCD cells cultured within engineered PEG-4MAL hydrogel and in the presence of an MT1-MMP inhibitor (Anti-MT1-



MMP antibody) or vehicle control (0.05% sodium azide). IMCD cell viability was assessed at 15 d after encapsulation. Bar, 200  $\mu$ m. (b) Percentage of IMCD multicellular structures (mean  $\pm$  SEM) that classified as “smooth clusters”, “spiked clusters”, or “tubules” after 15 d of encapsulation. At least 10 multicellular structures were analyzed per condition. (c) Fluorescence microscopy images of IMCD cells cultured within engineered PEG-4MAL hydrogel stained for actin (phalloidin), nuclei (DAPI) and expression of MT1-MMP. Relative fluorescence intensity analysis was performed on MT1-MMP images. Bars, 50  $\mu$ m. (b)  $\chi^2$  test with Bonferroni’s correction was used; \*,  $P < 0.0001$  for Control vs 10  $\mu$ M, and Control vs 30  $\mu$ M Anti-MT1-MMP antibody. An adjusted p-value  $< 0.05$  was considered significant. Experiments performed with 6 PEG-4MAL hydrogels per experimental group. Three independent experiments were performed and data are presented for one of the experiments.

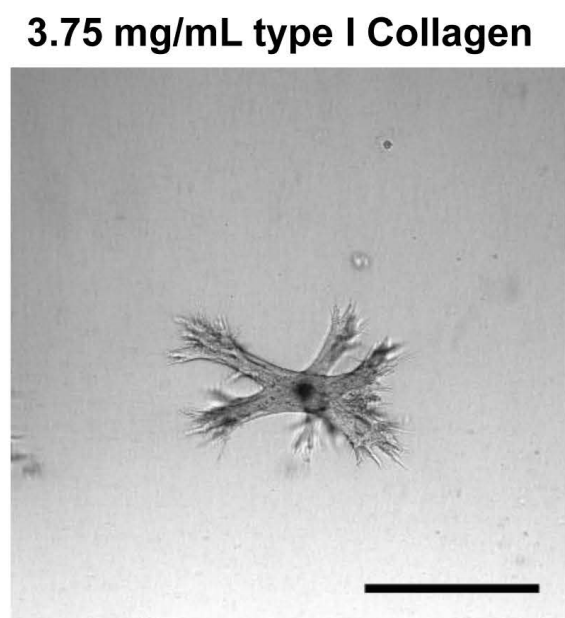
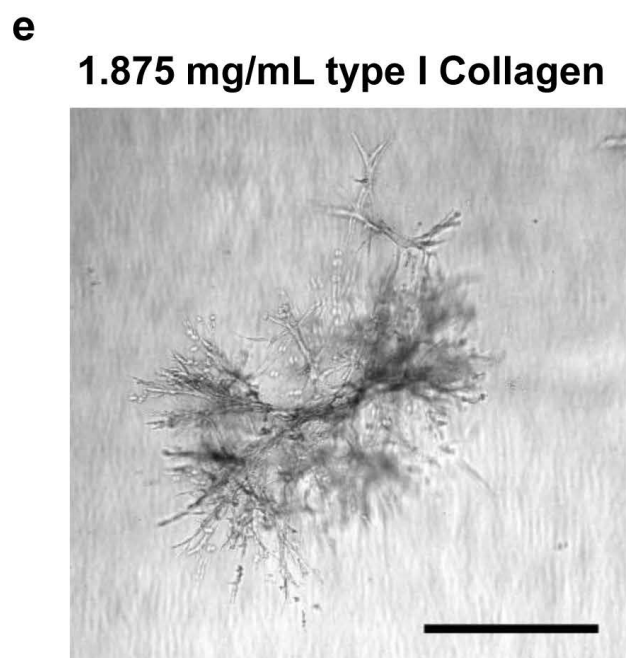
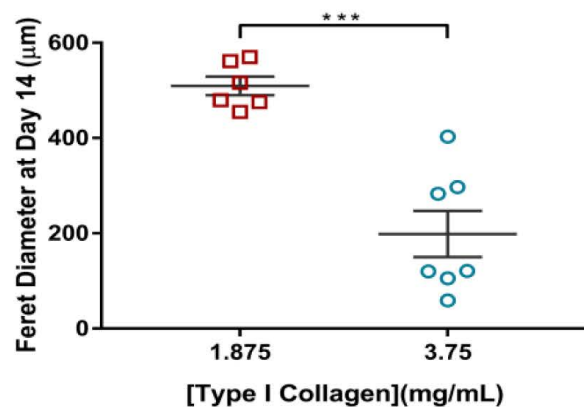
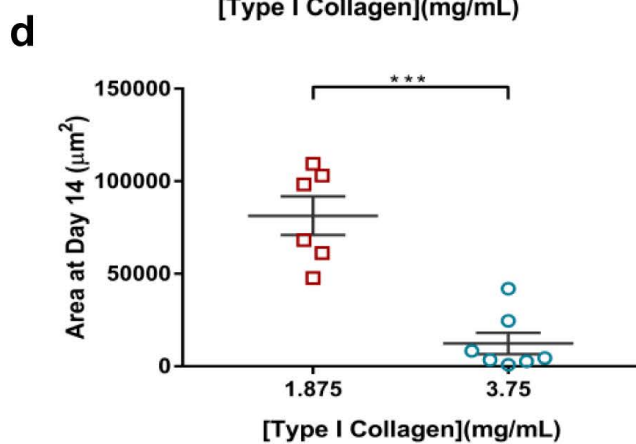
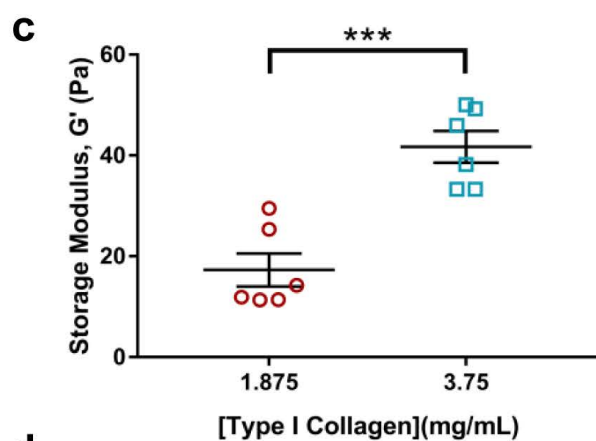
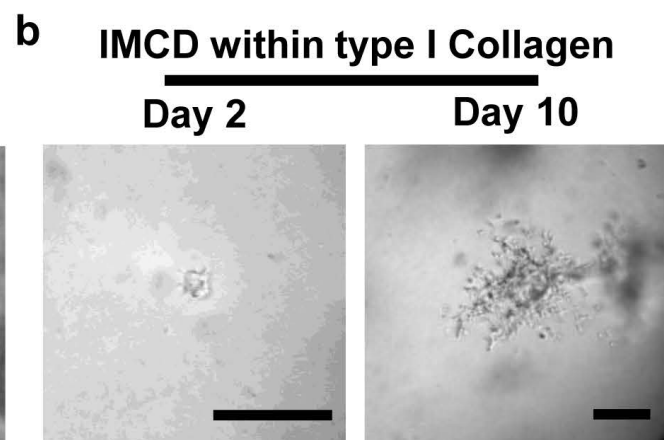
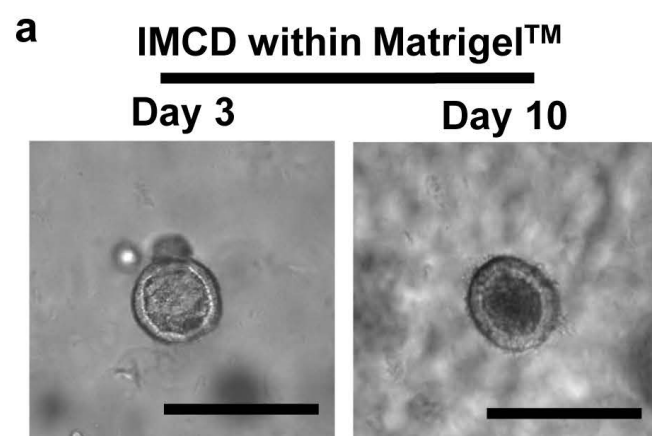


**Figure S1: Epithelial IMCD cells form multicellular tubular structures within Matrigel™ and type I collagen gels.** (a) IMCD cells within Matrigel™ proliferate to form multicellular spheroidal structures over time. (b) IMCD cells within type I collagen gels proliferate to form multicellular tubular structures over time. (c) Relationship between type I collagen density (mg/mL) and storage modulus (mean  $\pm$  SEM). (d) IMCD multicellular structure projected area and Feret diameter at 14 d after encapsulation in type I collagen gel. Each data point represents one (c) collagen gel or (d) multicellular structure. Graph lines represent the mean of the individual data points. Unpaired t-test with Welch's correction was used. P-values of statistical significance are represented as \*\*\* $P < 0.0002$ . An adjusted p-value  $< 0.05$  was considered significant. (e) Transmitted light microscopy images of IMCD cells within type I collagen gels of different concentrations after 14 d post-encapsulation. Bars, 100  $\mu$ m. Experiments performed with 6 collagen gels or Matrigel™ per experimental group.

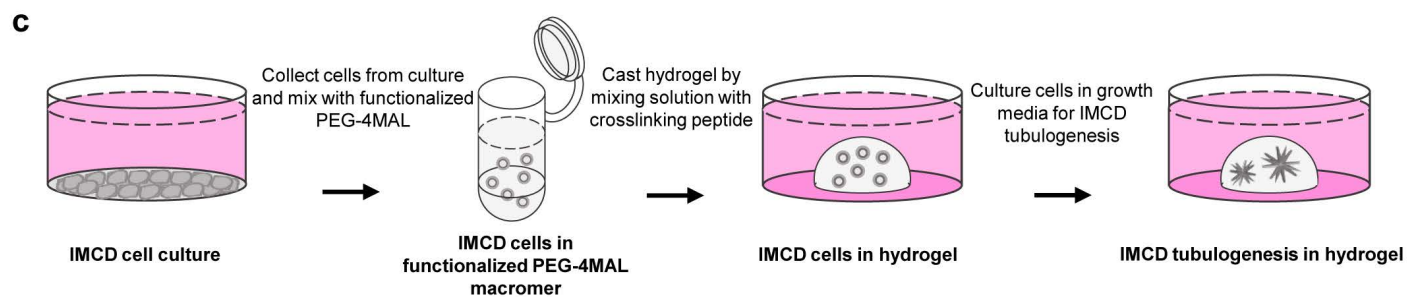
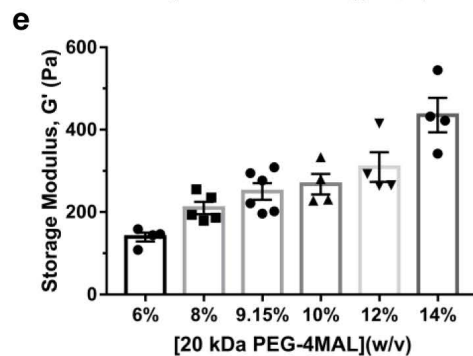
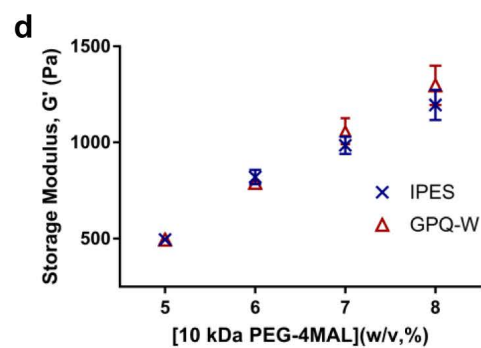
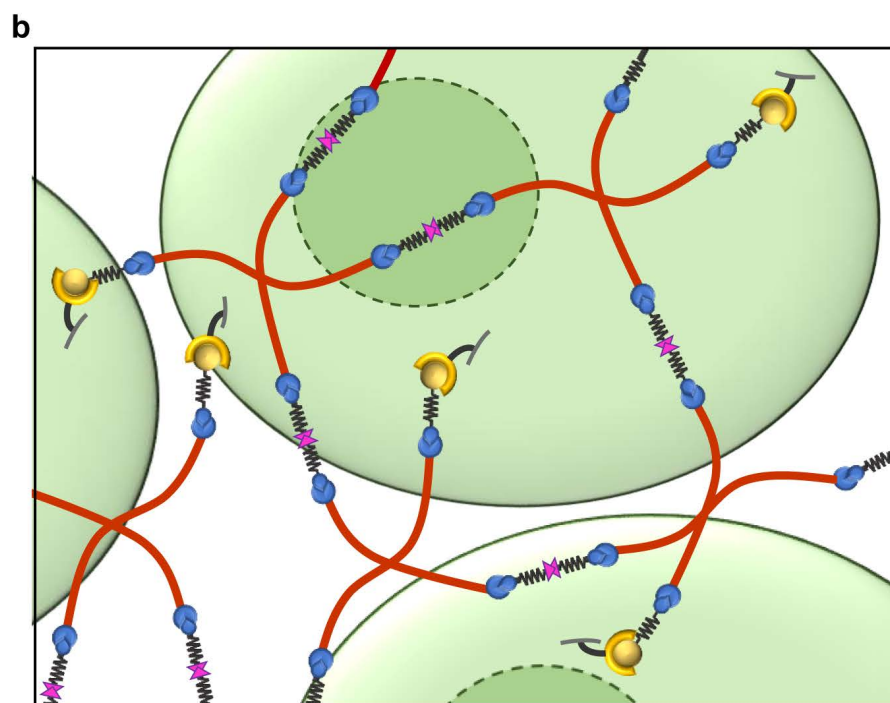
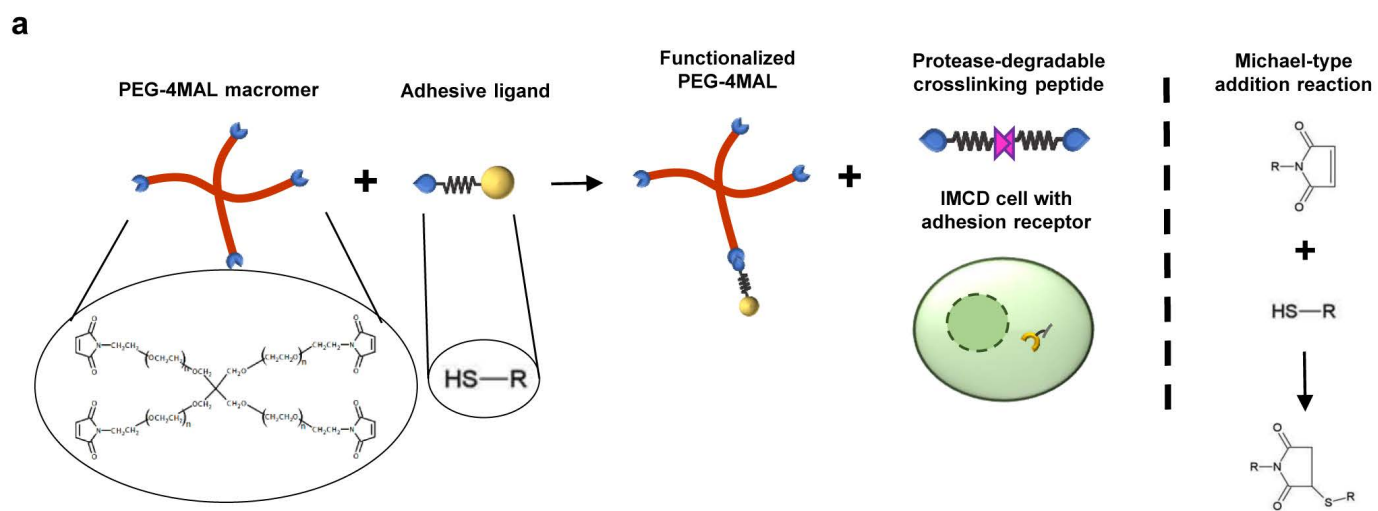


**Figure S2: PEG-4MAL hydrogel preparation and mechanical properties.** (a) PEG-4MAL macromers are conjugated with thiol-containing adhesive peptide to produce a functionalized PEG-4MAL macromer via Michael-type addition reaction, which is then crosslinked in the presence of cells using protease-cleavable peptides containing terminal cysteines to form (b) a hydrogel network. (c) IMCD cells are collected from culture plates and mixed with functionalized PEG-4MAL macromer solution, subsequently cast in multi-well plates and cultured in growth media to obtain IMCD tubules. (d) Relationship between polymer density (wt%) and storage modulus (mean  $\pm$  SEM) of 10 kDa PEG-4MAL hydrogels functionalized with 2 mM RGD and crosslinked with GPQ-W or IPES. (e) Relationship between polymer density (wt%) and storage modulus (mean  $\pm$  SEM) of 20 kDa PEG-4MAL hydrogels functionalized with 2 mM (for 6, 8, 10, 12 and 14%) or 4 mM RGD (for 9.15%) and crosslinked with IPES. Each data point represents an independently prepared hydrogel. Analysis performed to at least 4 PEG-4MAL hydrogels per experimental group. Adapted from Cruz-Acuña and Quirós et al. (2017).

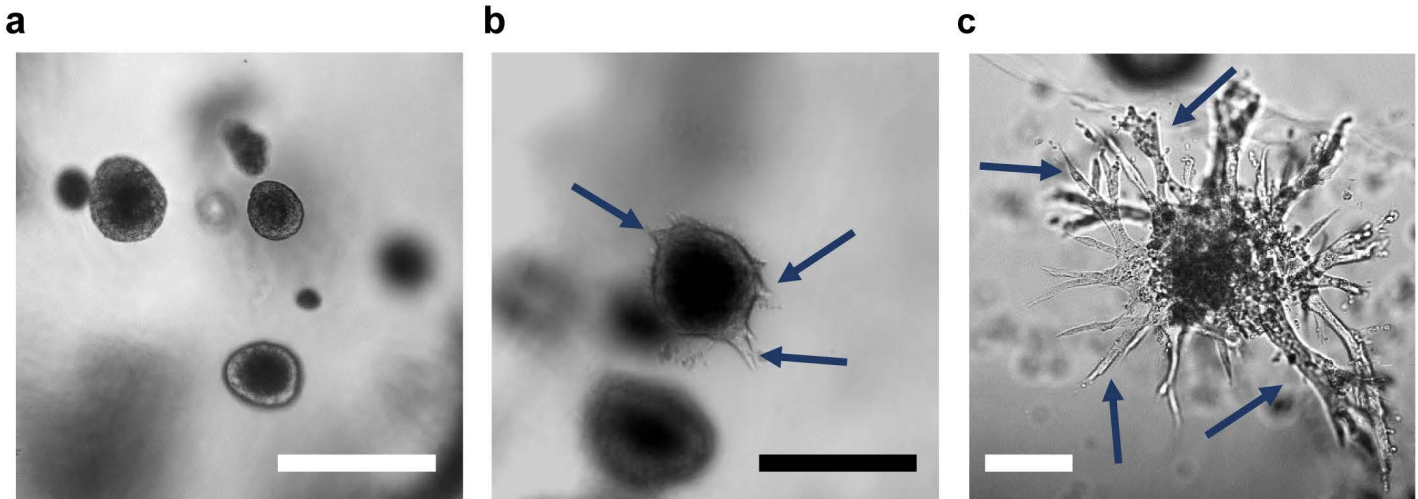


**Figure S3: PEG-4MAL hydrogel promotes formation of IMCD multicellular structures of different phenotypes.** Transmitted light microscopy images of IMCD multicellular structures within PEG-4MAL hydrogels forming (a) smooth cluster, (b) spiked clusters, or (c) tubules after 21 d post-encapsulation. Blue arrows indicate (b) spikes or (c) tubules in multicellular IMCD structures. Bars, 100  $\mu\text{m}$ .

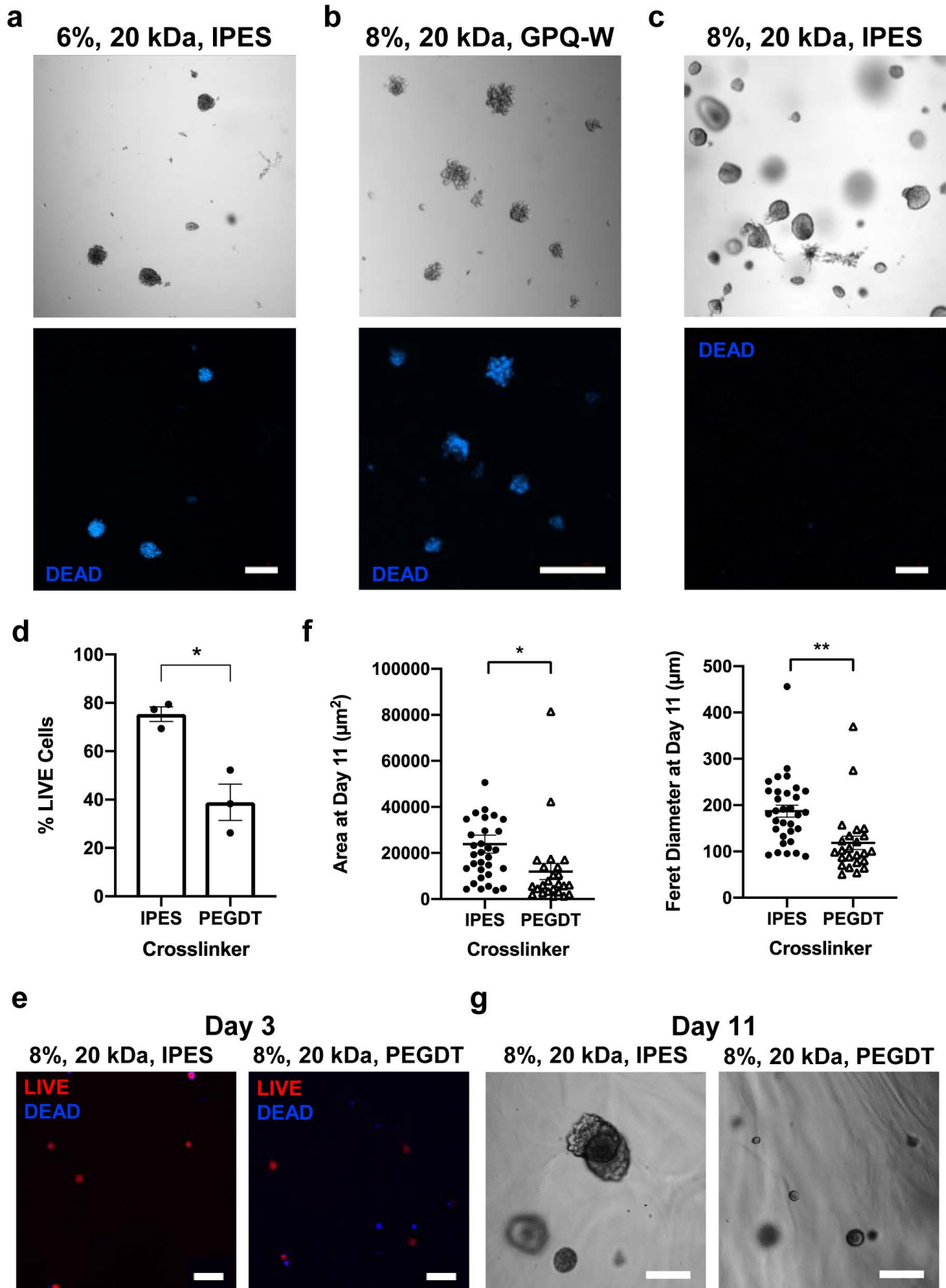




**Figure S4: Threshold level of PEG-4MAL mechanical properties and matrix degradability dictates IMCD cell viability.** (a-c) Transmitted light and fluorescence microscopy images of IMCD cells cultured in PEG-4MAL hydrogels of different conditions stained for dead. IMCD cell viability was assessed at 7 d after encapsulation on (a) 6%, 20 kDa PEG-4MAL-RGD hydrogels crosslinked with IPES peptide, or (b) 8%, 20 kDa PEG-4MAL-RGD hydrogels crosslinked with GPQ-W peptide, or (c) 8%, 20 kDa PEG-4MAL-RGD hydrogels crosslinked with IPES peptide. (d) Percentage of IMCD cells that stained for live (mean  $\pm$  SEM) after 3 d of encapsulation in 8%, 20 kDa PEG-4MAL-RGD hydrogels crosslinked with IPES peptide or non-degradable PEGDT. (e) Fluorescence microscopy images of IMCD cells cultured in PEG-4MAL hydrogels. IMCD cell viability was assessed at 3 d after encapsulation. (f) IMCD multicellular structure projected area and Feret diameter at 11 d after encapsulation in 8%, 20 kDa PEG-4MAL-RGD hydrogels crosslinked with IPES peptide or PEGDT. (g) Transmitted light microscopy images of IMCD cells cultured in PEG-4MAL hydrogels. Bars, 200  $\mu$ m. Graph line represents the mean of the individual data points. Each data point represents one multicellular structure. Unpaired t-test with Welch's correction was used. P-value of statistical significance is represented as \*\*P < 0.0021, \*P < 0.0332. An adjusted p-value < 0.05 was considered significant. Experiments performed with 6 PEG-4MAL hydrogels per experimental group.

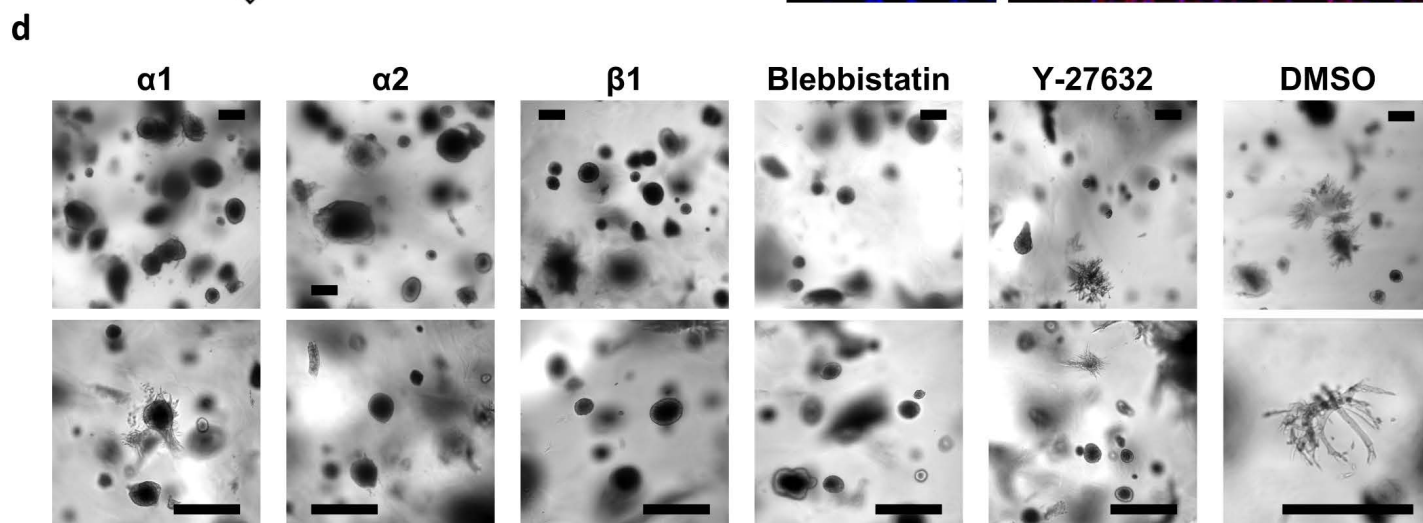
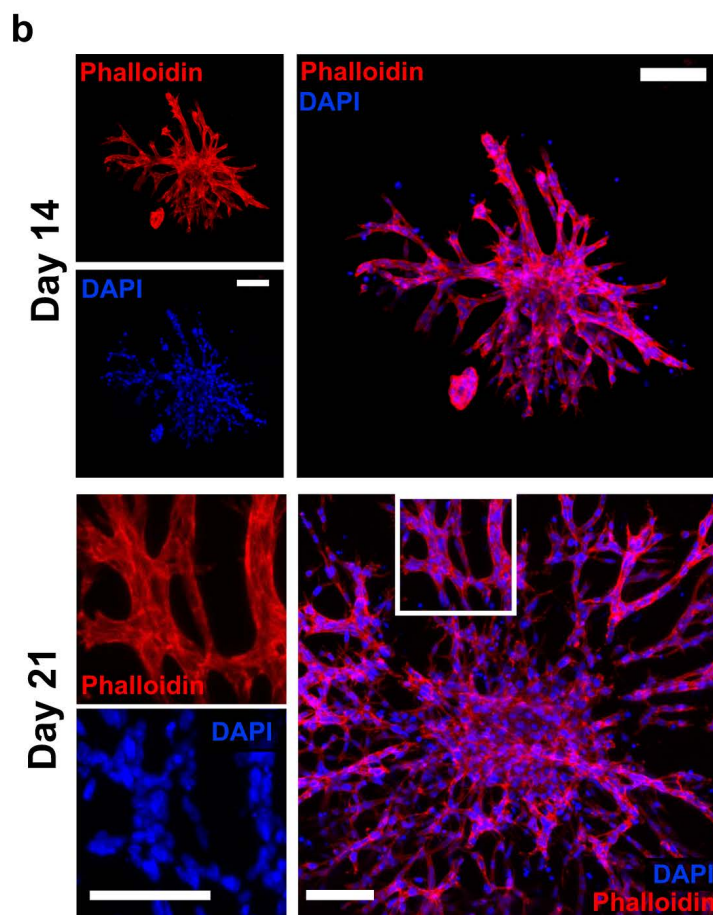
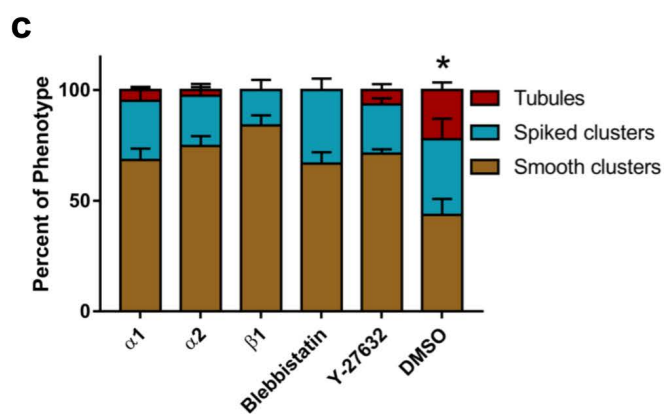
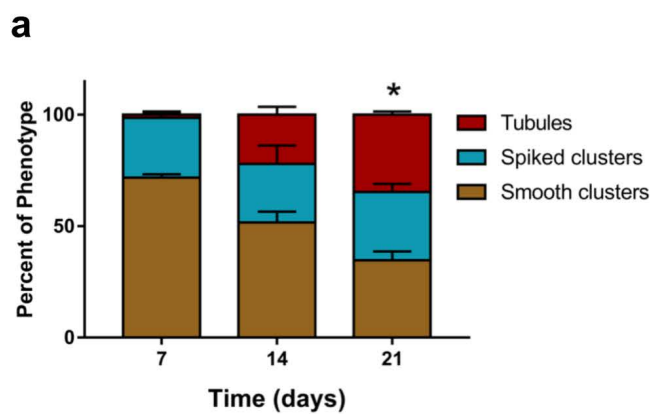


**Figure S5: Engineered PEG-4MAL hydrogel promotes increase in the number of multicellular structures with organized tubules over time via integrin receptors and cellular contractility.** (a) Percentage of IMCD multicellular structures (mean  $\pm$  SEM) that classified as either “smooth clusters”, “spiked clusters”, or “tubules” after 7, 14 and 21 d of encapsulation in the engineered hydrogel.  $\chi^2$  test with Bonferroni’s correction was used; \*,  $P < 0.0001$  for day 7 vs day 21. At least 10 multicellular structures were analyzed per condition. (b) Fluorescence microscopy images of IMCD tubules within engineered hydrogel stained for actin (phalloidin) and nuclei (DAPI) at different time-points. Bars, 100  $\mu\text{m}$ . (c) Percentage of IMCD multicellular structures (mean  $\pm$  SEM) that classified as either “smooth clusters”, “spiked clusters”, or “tubules” after 21 d of encapsulation in the engineered hydrogel and in the presence of inhibitors of integrin subunits and cellular contractility.  $\chi^2$  test with Bonferroni’s correction was used; \*,  $P < 0.0002$  for DMSO vs  $\alpha_1$ ,  $P < 0.0002$  for DMSO vs  $\alpha_2$ ,  $P < 0.0001$  for DMSO vs  $\beta_1$ ,  $P < 0.0002$  for DMSO vs blebbistatin, and  $P < 0.0012$  for DMSO vs Y-27632. At least 10 multicellular structures were analyzed per condition. A p-value  $< 0.0332$  was considered significant. (d) Transmitted light images of IMCD multicellular structures at 21 d post encapsulation in the engineered hydrogel in the presence of inhibitors of integrin subunits and cellular contractility. Bars, 200  $\mu\text{m}$ . Experiments performed with 6 PEG-4MAL hydrogels per experimental group.

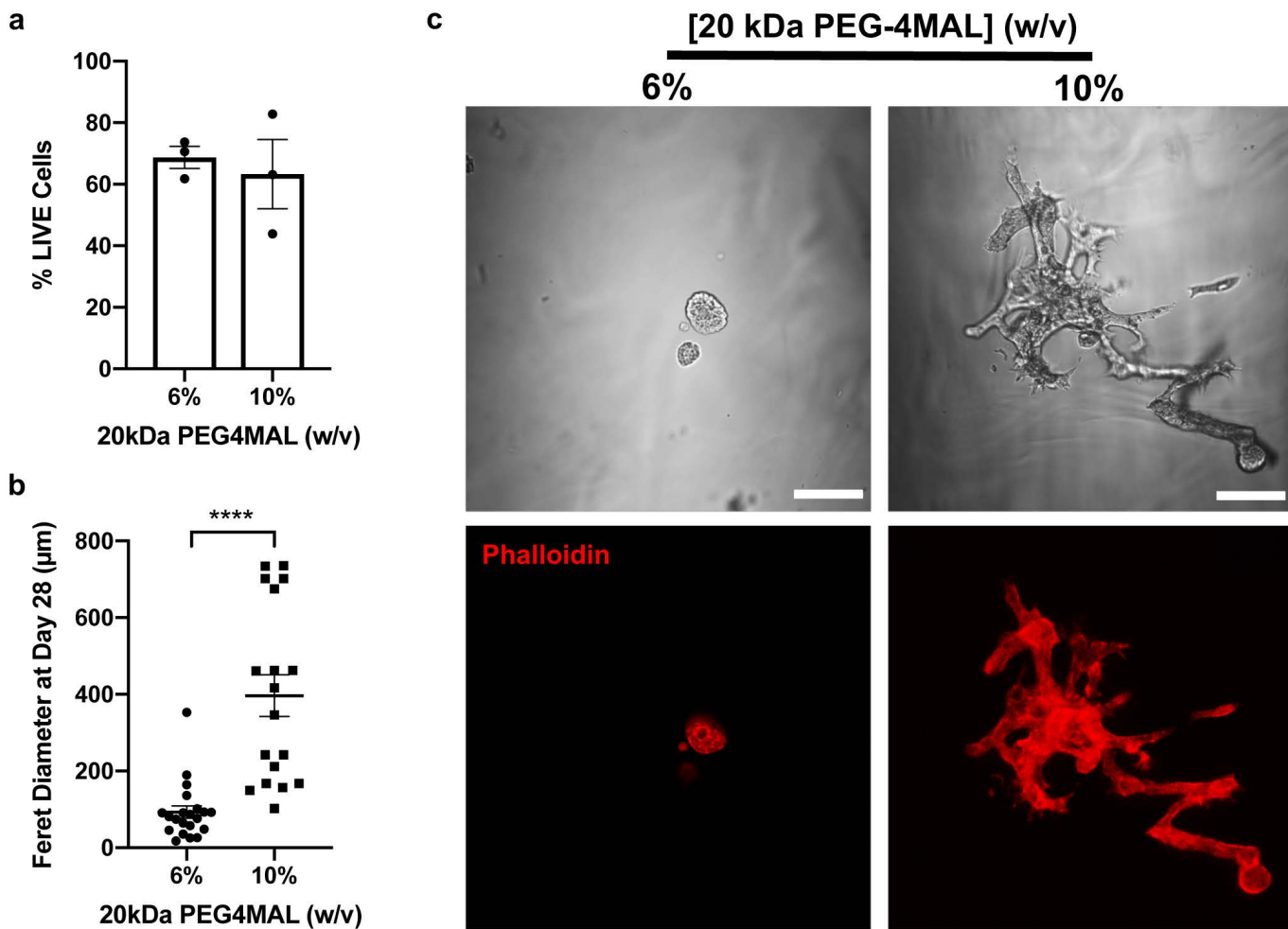


**Figure S6: Engineered PEG-4MAL hydrogel supports tubulogenesis of primary renal proximal tubule cells.** (a) Percentage of RPTCs that stained for live (mean ± SEM) after 1 d of encapsulation in 6% and 10% PEG-4MAL-RGD hydrogels crosslinked with IPES peptide. Each data point represents one independent hydrogel. At least 100 cells were assessed per condition. (b) RPTC multicellular structure Feret diameter at 28 d after encapsulation in PEG- 4MAL hydrogels. Each data point represents one multicellular structure. Graph lines represent the mean of the individual data points. Unpaired t-test with Welch's correction was used. P-value of statistical significance is represented as \*\*\*\*P < 0.0001. An adjusted p-value < 0.05 was considered significant. (c) Transmitted light and fluorescence microscopy images of RPTCs at 28 d after encapsulation in PEG-4MAL hydrogels stained for actin (phalloidin). Bar, 100 μm. Experiments performed with 6 PEG-4MAL hydrogels per experimental group.